Available online at http://scik.org
Commun. Math. Biol. Neurosci. 2023, 2023:12
https://doi.org/10.28919/cmbn/7875
ISSN: 2052-2541

# ON THE FRACTIONAL-ORDER MODELING OF COVID-19 DYNAMICS IN A POPULATION WITH LIMITED RESOURCES

J. O. AKANNI[1,2], FATMAWATI[2,*], C. W. CHUKWU[3]

[1]Department of Mathematical and Computing Sciences, Koladaisi University, Ibadan, Oyo State, Nigeria

[2]Department of Mathematics, Faculty of Science and Technology, Universitas Airlangga, Surabaya, Indonesia

[3]Department of Mathematics, Wake Forest University, Winston-Salem, NC 27109, USA



**Abstract.** Resource availability plays a pivotal role in the fight against emerging infections such as COVID-19. In the event where there are limited resources the control of an epidemic disease tends to be slow and the disease spread faster in the human population. In this paper, we are motivated to formulate and investigate a mathematical model via the Caputo derivative which incorporates the impact of limited resources on COVID-19 transmission dynamics in the population. We analyze the fractional model by computing the equilibrium points, and basic reproduction number, $(\mathscr{R}_0)$, and also used the Banach-fixed point theorem to prove the existence and uniqueness of the solution of the model. The impact of each parameter on the dynamical spread of COVID-19 was examined by the help of Sensitivity analysis. Results from mathematical analyses depict that the disease-free equilibrium is stable if $\mathscr{R}_0 < 1$ and unstable otherwise. Numerical simulations were carried out at different fractional order derivatives to understand the impact of several model parameters on the dynamics of the infection which can be used to establish the influential parameter driving the epidemic transmission path. Our numerical results show that an increase in the recovery rate of hospitalization increases the number of infected individuals. The results of this work can help policymakers to devise strategies to reduce the COVID-19 infection.

**Keywords:** COVID-19; fractional model; Caputo operator; limited resources; stability analysis; sensitivity analysis.

**2020 AMS Subject Classification:** 34A08, 92B05.

*Corresponding author

E-mail address: fatmawati@fst.unair.ac.id.

Received January 5, 2023

## 1. INTRODUCTION

Severe acute respiratory syndrome (SARS) first occurred in the year 2002-2003 in Guangdong Province, China [1]. In 2015, South Korea experienced a similar outbreak known as the Middle East respiratory syndrome (MERS) [2, 3]. On the other hand, in Wuhan, China, a disease called SARS Coronavirus 2 (SARS-CoV-2) which is a new type of variant coronavirus emerged in December 2019 [4]. The world health organization (WHO) later declared it a pandemic on 11 March 2020 [5]. This disease can transmit directly from human to human or through contact with contaminated surfaces, coughing or sneezing [6, 7] while the asymptomatic stage of the infection can last for up to 14 days before becoming infectious. The infected individuals at this stage show passive symptoms ranging from respiratory infection like coughing and wheezing which can later to an inability to smell and loss of taste [7]. While the elderly and those with underlining illness such as diabetes, obesity, and hypertension easily succumb to the disease [8, 9, 10, 11]. Currently, the world has recorded a total of 612,076,308 coronavirus cases with about 6,509,597 deaths and 589,858,670 recovered individuals until date [12].

The alarming rate of COVID-19 cases and mortality has caused a global health concern. Several control measures such as social distancing, wearing masks, regular hand washing, the use of hand sanitizers, social distancing, isolation of infected people, bans on air travel, and social gatherings in different areas were implemented at the early stage of the pandemic to reduce the total number of infections. Additionally, various countries and regions of the world enforced lockdowns in the most affected areas to help control the spread of the virus and halt the chain of transmission caused by the infectious individuals in the whole susceptible population [13].

Mathematical modeling has played a vital role in predicting several ways that enable most world governments to mitigate the spread of the disease. Most of these models included using a statistical approach, agent-based modeling, and ordinary differential equations consisting of integer and non-integer order models to quantify the COVID-19 transmission and beneficial ways to mitigate the infection. See the following published literature which has implemented the integer order model [14, 15, 16, 17, 18, 19, 20, 21]. Fractional calculus has shown to have a memory effect that gives more accurate results in forecasting physical systems including

mathematical models [22]. This has led to new advancements in developing new fractional-order operators namely Riemann-Liouville, Caputo, Caputo–Fabrizio, and Atangana–Baleanu utilized in solving both integer and non-integer orders systems of differential equations arising from real-world problems such as applications to integrodifferential equations [23, 24], mathematical epidemiology [25, 26], economic and financial [27, 28] and many other fields. On the other hand, fractional order, which consists of Caputo fractional and Atangana-Balenu (ABC) derivatives, has also been applied in modeling the spread of COVID-19 as in [29, 30, 31]. We now focus on reviewing some of the above-mentioned literature. The work in [30] used a Caputo model to study COVID-19 in Indonesia, considering environmental transmission and vaccination. The results from numerical simulations of their model show that the spread of SARS-CoV-2 greatly depends on the contact rate of the virus transmission. While in contrast, the vaccination rate impacted negatively on the model basic reproduction number and similarly the number of infected individuals in the population. Li *et al.* [22] implemented a fractional piece-wise Caputo and Atangana–Baleanu–Caputo (ABC) model which examined the effect of COVID-19 Omicron variant fitted to South Africa COVID-19 epidemiological data set and found that adherence to non-pharmaceutical interventions such as social distances, wearing face masks, avoiding social gatherings will have a negative effect on the number of infected case in the third wave of the pandemic in the case of South Africa COVID epidemic course. Furthermore, Ahmad *et al.* [32] used an ABC fractional derivative to study the impact of quarantine and social distancing on the COVID-19 epidemic. It is found that the best method to stop the spread of the virus is to social distance in the form of staying at home which can be ahead through lockdown implementation, in contrast, the infected individuals should isolate to avoid an increase in disease transmission. Also, Shah *et al.* [8] formulated a non-integer order model for COVID-19 dynamics. The reproduction number was calculated and the asymptotic stability of the proposed model was examined. It was found that the numerical simulation is in good agreement with the theoretical results. The fractional order differential equations were used by Atangana [24] to study the spread of COVID-19.

Cakan [16] used an *SEIR* model to study the impact COVID-19 in the presence of limited resources considering the hospital setting. Their findings suggest that higher contact rates between susceptible and infected individuals lead to higher hospitalized individuals, which can grow beyond the carrying capacity of the present hospitals. Authors believe that the lack of adequate resources to control such kind of virus contributed to a large number of cases of the COVID-19 pandemic across the globe [12]. In this study, a new mathematical model for the COVID-19 outbreak by incorporating limited resources is extended into a fractional-order model in the sense of the Caputo fractional derivative. We modified the basic epidemic model with limited public health resources as extended by [33, 34]. Using the idea of the fractional ordinary differential equation, we are thinking that the fractional-order model will accommodate the real phenomenon of the spread of COVID-19. Similarly, the results of this model will help policymakers to devise strategies to reduce the COVID-19 infection. In the next section, we present preliminaries for the fractional Caputo derivative.

## 2. BASICS OF FRACTIONAL CALCULUS

This section presents brief essential definitions regarding fractional calculus in Caputo sense.

**Definition 1** (see [35]). Consider $y \in \mathscr{C}^n$ be function, then Caputo derivative having fractional order $\alpha$ in $(n-1,n)$ where $n \in \mathbb{N}$ is defined as:

$$ {}^{C}D_t^{\alpha}(f(t)) = \frac{1}{\Gamma(n-\alpha)} \int_0^t (t-s)^{(n-\alpha-1)} f^{(n)}(s) ds, \tag{1}$$

with $\Gamma(.)$ is the gamma function and ${}^{C}D_t^{\alpha}(f(t))$ tends to $f^{'}(t)$ as $\alpha \longrightarrow 1$.

**Definition 2** (see [35]). The Corresponding integral with fractional order $\alpha > 0$ of the function f:$\mathbb{R}^+ \longrightarrow \mathbb{R}$ is expressed as follows:

$$ I_t^{\alpha}(f(t)) = \frac{1}{\Gamma(\alpha)} \int_0^t (t-s)^{(\alpha-1)} f(s) ds,\ 0 < \alpha < 1,\ t > 0. \tag{2}$$

**Definition 3**. Let $y^*$ denote the equilibrium of the Caputo fractional model then:

$$ {}^{C}D_t^{\alpha}(f(t)) = h(t, f(t)),\ \alpha \in (0,1),\ iff\ h(t, f^*) = 0. \tag{3}$$

## 3. Model Formulation

This section evaluates the formulation of an epidemic model of COVID-19 disease in a community with insufficient aids. Thus, the community denoted as N(t), is distributed into six mutually exclusive components, i.e., susceptible class, $S(t)$ (individuals who are likely to contract COVID-19), exposed class, $E(t)$ (those who are infected but not infectious yet), quarantined class, $Q(t)$ (those who are in isolation center or self-isolation), infectious class, $I(t)$ (those who display the symptoms and are capable of the disease spread), $H(t)$ (those who are infectious and admitted to a health care facility) and recovered class, $R(t)$ (those who have recovered from COVID-19 infection). Thus,

$$N(t) = S(t) + E(t) + Q(t) + I(t) + H(t) + R(t). \tag{4}$$

In order to understand the effect of the capacity and inadequate comprehend the effect of the capability and inefficient health structures, the recovery rate for people in class $H$ integrating the effect of capacity and inefficient health facilities is developed as a nonlinear function as

$$\sigma = \sigma(b,H) = \sigma_0 + (\sigma_1 - \sigma_0)\frac{b}{H+b}, \tag{5}$$

where $b > 0$ represents the hospital bed-population ratio, $\sigma_0$ is the minimum per capita recovery rate owing to the function of the basic healthcare system, and $\sigma_1$ accounts for the maximum per capita recovery rate corresponding to the sufficient clinical resources and few hospitalized humans. A similar function to the ones given in (5) was previously suggested in [33, 34]. Consequently, the model governing the COVID-19 dynamics in the population according to the flowchart illustrated in Figure 1 is derived as

$$\begin{aligned}
\frac{dS}{dt} &= \Lambda + \rho Q - \frac{\beta S(I+\varepsilon H)}{N} - \mu S - d_0 S,\\
\frac{dE}{dt} &= \frac{\beta S(I+\varepsilon H)}{N} - (\delta + \psi + d_0)E,\\
\frac{dQ}{dt} &= \mu S + \delta E - (h_2 + \rho + d_0)Q,\\
\frac{dI}{dt} &= \psi E - (h_1 + d_0 + d_1)I,\\
\frac{dH}{dt} &= h_1 I + h_2 Q - (\sigma(b,H) + d_0 + d_1)H,\\
\frac{dR}{dt} &= \sigma(b,H)H - d_0 R.
\end{aligned} \tag{6}$$

The explanation of the parameters used in model (6) is provided in Table 1, while the scheme of the model is as shown in Figure 1.

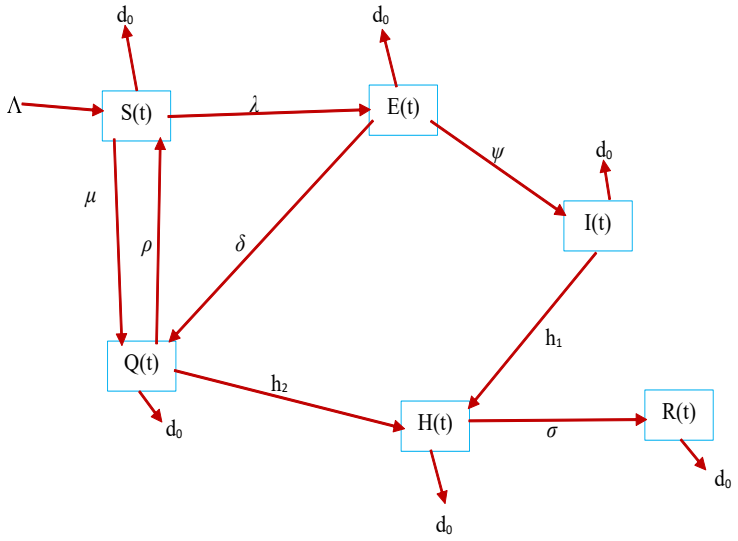


FIGURE 1. Flowchart of model (6) with $\lambda = \frac{\beta S(I+\varepsilon H)}{N}$

TABLE 1. Definition of each parameter of model (6).

| Parameter | Description |
|---|---|
| $\Lambda$ | Recruitment rate |
| $d_0$ | Natural death rate |
| $\beta$ | Effective transmission rate |
| $d_1$ | COVID-19-induced death rate |
| $\psi$ | Disease progression rate of the exposed class |
| $\sigma$ | Per capita recovery rate for hospitalized individuals |
| $\mu$ | Progression rate of individuals in class $S$ to class $Q$ |
| $\varepsilon$ | Modification parameter relative infectious individuals in class $H$ |
| $\delta$ | Detection rate at which exposed individuals become quarantined |
| $h_1(h_2)$ | Hospitalization rates for infectious (quarantined) individuals respectively |
| $\rho$ | Rate at which quarantined individuals become susceptible |

**3.1. Positivity of Solutions.** We prove that all the variables remain non-negative and the solutions of model (6) with positive initial values will remain positive for all $t > 0$. We thus provide the following theorem.

**Theorem 1** *Given that the initial values of the model* (6) *are* $S(0) > 0$, $E(0) > 0$, $Q(0) > 0$, $I(0) > 0$, $H(0) > 0$ *and* $R(0) > 0$. *There exists* $(S(t),E(t),Q(t),I(t),H(t),R(t)) : (0,\infty) \longrightarrow (0,\infty)$ *which solves model.*(6)

*Proof.* Assume that $\hat{t}$=sup$\{t > 0 : S(0) > 0, E(0) > 0, Q(0) > 0, I(0) > 0, H(0) > 0\} \in [0,t]$. Thus $\hat{t} > 0$, and it follows from the first equation of model (6) that

$$\frac{dS}{dt} \geq -(\lambda + \mu + d_0)S$$

where $\lambda = \frac{\beta(I+\varepsilon H)}{N}$, we thus have

$$\frac{d}{dt}\left[S(t)exp\left((\mu + d_0)t + \int_0^t \lambda(\tau)d\tau\right)\right] \geq 0,$$

resulting to,

$$S(t) \geq S(0)exp\left(-\left((\mu + d_0)t + \int_0^t \lambda(\tau)d\tau\right)\right) > 0, \forall\, t > 0.$$

In a similar fashion it can also be exhibited that $E(0) > 0$, $Q(0) > 0$, $I(0) > 0$, $H(0) > 0$ and $R(0) > 0$ for all $t > 0$, and this completes the proof. □

**3.2. Invariant region.** This Section present the point at which the model (6) will be positively invariant.

**Theorem 2** *Let* ($S(t)$, $E(t)$, $Q(t)$, $I(t)$, $H(t)$ *and* $R(t)$) *be the solution of system* (6) *with initial values* $S(0)$, $E(0)$, $Q(0)$, $I(0)$, $H(0)$ *and* $R(0)$. *The compact set,*

$$\Phi = \left\{(S,E,Q,I,H,R) \in \mathbb{R}^9_+ : N \leq \frac{\Lambda}{d_0}\right\}$$

*is positively invariant and attracts all solutions in* $\mathbb{R}^6_+$

*Proof.* We attend the proof presented in [36, 37]. Based on the equation (6), the time derivative of $N(t)$ is assigned by

$$
\begin{aligned}
\frac{dN}{dt} &= \frac{dS}{dt}+\frac{dE}{dt}+\frac{dQ}{dt}+\frac{dI}{dt}+\frac{dH}{dt}+\frac{dR}{dt},\\
&= \Lambda - d_0 N - d_1(I+H) \leq \Lambda - d_0 N \qquad (7)\\
N &\leq \frac{\Lambda}{d_0}.
\end{aligned}
$$

From (7) we have $\frac{dN}{dt} \leq 0$ which implies that $\Phi$ is a positively invariant set. We also note that by solving (7) we have

$$0 \leq N(t) \leq \left(\frac{\Lambda}{d_0} + N(0)e^{-\mu t}\right),$$

where $N(0)$ is the initial condition of $N(t)$. Thus, $0 \leq N(t) \leq \frac{\Lambda}{d_0}$ as $t \longrightarrow \infty$ and hence $\Phi$ is an attractive set. □

## 4. FRACTIONAL-ORDER MODEL

This section evaluates a fractional-order COVID-19 model (6). The fractional model appropriating to the system (6) is illustrated below:

$$
\begin{aligned}
{}^{C}D^{\alpha}_{0,t}S(t) &= \Lambda + \rho Q - \frac{\beta S(I+\varepsilon H)}{N} - \mu S - d_0 S,\\
{}^{C}D^{\alpha}_{0,t}E(t) &= \frac{\beta S(I+\varepsilon H)}{N} - (\delta + \psi + d_0)E,\\
{}^{C}D^{\alpha}_{0,t}Q(t) &= \mu S + \delta E - (h_2 + \rho + d_0)Q, \qquad (8)\\
{}^{C}D^{\alpha}_{0,t}I(t) &= \psi E - (h_1 + d_0 + d_1)I,\\
{}^{C}D^{\alpha}_{0,t}H(t) &= h_1 I + h_2 Q - (\sigma(b,H) + d_0 + d_1)H,\\
{}^{C}D^{\alpha}_{0,t}R(t) &= \sigma(b,H)H - d_0 R.
\end{aligned}
$$

where $\alpha$ in $0 < \alpha \leq 1$ represents the order of the fractional derivative. The fractional derivative of the model (8) is in the significance of Caputo. The Caputo method is mainly utilized in actual applications. The major benefits of the Caputo approach are the introductory values for the fractional differential equations putting up with the same establishment as for integer order differential equations [35]. The Caputo fractional derivative is interpreted below.

*Corollary 1.* Suppose, $g(x) \in C[a_1, B_1]$ and ${}^{C}D^{\alpha}_{t}y(x) \in a_1 < \alpha \leq b_1$, where $\alpha \in 0 < \alpha \leq 1$. Then if

(i). ${}^{C}D_{t}^{\alpha}y(x) \geq 0, \forall\, x \in (a_1, b_1)$, then $y(x)$ is increasing.

(ii). ${}^{C}D_{t}^{\alpha}y(x) \leq 0, \forall\, x \in (a_1, b_1)$, then $y(x)$ is decreasing.

**4.1. Fractional model analysis.** In this subsection, some fundamental and essential mathematical elements of the proposed model (8) are presented.

**4.1.1.** *Existence and uniqueness of the model solution.* This section examines the presence and essence of the solution for the Caputo operator with the aid of fixed point theory. For this, let $\mathscr{B}(\mathscr{X})$ indicate a Banach space comprises real-valued continual functions over the interval $\mathscr{X} = [0, a]$ with norm interpreted by $\|S\| = sup_{t\in\mathscr{G}}|S(t)|$, $\|E\| = sup_{t\in\mathscr{G}}|E(t)|$, $\|Q\| = sup_{t\in\mathscr{G}}|Q(t)|$, $\|I\| = sup_{t\in\mathscr{G}}|I(t)|$, $\|H\| = sup_{t\in\mathscr{G}}|H(t)|$, $\|R\| = sup_{t\in\mathscr{G}}|R(t)|$, and the norm $\|(S,E,Q,I,H,R)\| = \|S\| + \|E\| + \|Q\| + \|I\| + \|H\| + \|R\|$.

*Proof.* The followings were obtained after using Caputo integral on system (8)

$$
\begin{aligned}
S(t) &= S(0) \ + \ {}^{C}I_{0,t}^{\alpha}S(t)\left\{\Lambda + \rho Q - \frac{\beta S(I+\varepsilon H)}{N} - \mu S - d_0 S\right\},\\
E(t) &= E(0) \ + \ {}^{C}I_{0,t}^{\alpha}E(t)\left\{\frac{\beta S(I+\varepsilon H)}{N} - (\delta + \psi + d_0)E\right\},\\
Q(t) &= Q(0) \ + \ {}^{C}I_{0,t}^{\alpha}Q(t)\left\{\mu S + \delta E - (h_2 + \rho + d_0)Q\right\},\\
I(t) &= I(0) \ + \ {}^{C}I_{0,t}^{\alpha}I(t)\left\{\psi E - (h_1 + d_0 + d_1)I\right\},\\
H(t) &= H(0) \ + \ {}^{C}I_{0,t}^{\alpha}H(t)\left\{h_1 I + h_2 Q - (\sigma(b,H) + d_0 + d_1)H\right\},\\
R(t) &= R(0) \ + \ {}^{C}I_{0,t}^{\alpha}R(t)\left\{\sigma(b,H)H - d_0 R\right\}.
\end{aligned}
\tag{9}
$$

Arising from definition (2), the following were obtained,

$$
\begin{aligned}
S(t) &= S(0) \ + \ \frac{1}{\Gamma(\alpha)}\int_0^t (t-\rho)^{\alpha-1}K_1(\rho, S(\rho))d\rho,\\
E(t) &= E(0) \ + \ \frac{1}{\Gamma(\alpha)}\int_0^t (t-\rho)^{\alpha-1}K_2(\rho, E(\rho))d\rho,\\
Q(t) &= Q(0) \ + \ \frac{1}{\Gamma(\alpha)}\int_0^t (t-\rho)^{\alpha-1}K_3(\rho, Q(\rho))d\rho,\\
I(t) &= I(0) \ + \ \frac{1}{\Gamma(\alpha)}\int_0^t (t-\rho)^{\alpha-1}K_4(\rho, I(\rho))d\rho,\\
H(t) &= H(0) \ + \ \frac{1}{\Gamma(\alpha)}\int_0^t (t-\rho)^{\alpha-1}K_5(\rho, H(\rho))d\rho,
\end{aligned}
\tag{10}
$$

$$R(t) = R(0) \; + \; \frac{1}{\Gamma(\alpha)} \int_0^t (t-\rho)^{\alpha-1} K_6(\rho, R(\rho)) d\rho.$$

The kernels are obtained as follows,

$$\begin{aligned}
K_1(t,S(t)) &= \Lambda + \rho Q - \frac{\beta S(I+\varepsilon H)}{N} - \mu S - d_0 S, \\
K_2(t,E(t)) &= \frac{\beta S(I+\varepsilon H)}{N} - (\delta + \psi + d_0)E, \\
K_3(t,Q(t)) &= \mu S + \delta E - (h_2 + \rho + d_0)Q, \\
K_4(t,I(t)) &= \psi E - (h_1 + d_0 + d_1)I, \\
K_5(t,H(t)) &= h_1 I + h_2 Q - (\sigma(b,H) + d_0 + d_1)H, \\
K_6(t,R(t)) &= \sigma(b,H)H - d_0 R.
\end{aligned} \tag{11}$$

All the equations in (11) satisfy the Lipschitz conditions with all the compartments possessing the upper limit. Suppose the functions $S(t)$ and $S^*(t)$ are considered, applying a similar approach for other functions, which gives rise to

$$\|K_1(t,S(t)) - K_1(t,S^*(t))\| = \|\frac{1}{N}(\beta S(I+\varepsilon H) + \mu + d_0)(S(t) - S^*(t))\|, \tag{12}$$

Let $g_1 = \|\frac{1}{N}(\beta S(I+\varepsilon H) + \mu + d_0)\|$. Using a similar approach, the remaining equations are obtained as follows

$$\begin{aligned}
\|K_1(t,S(t)) - K_1(t,S^*(t))\| &= g_1 \|(S(t) - S^*(t))\|, \\
\|K_2(t,E(t)) - K_2(t,E^*(t))\| &= g_2 \|(E(t) - E^*(t))\|, \\
\|K_3(t,Q(t)) - K_3(t,Q^*(t))\| &= g_3 \|(Q(t) - Q^*(t))\|, \\
\|K_4(t,I(t)) - K_4(t,I^*(t))\| &= g_4 \|(I(t) - I^*(t))\|, \\
\|K_5(t,H(t)) - K_5(t,H^*(t))\| &= g_5 \|(H(t) - H^*(t))\|, \\
\|K_6(t,R(t)) - K_6(t,R^*(t))\| &= g_6 \|(R(t) - R^*(t))\|.
\end{aligned} \tag{13}$$

where $g_1, g_2, g_3, g_4, g_5$ and $g_6$ denote the Lipschitz constants respectively which is corresponding to all the six kernels and by this, the Lipschitz condition is concerned satisfied. The algorithm of equations in (10) can be presented as follows:

$$
\begin{aligned}
S_n(t) &= S(0) + \frac{1}{\Gamma(\alpha)}\int_0^t (t-\rho)^{\alpha-1} K_1(\rho, S_{n-1}(\rho))d\rho,\\
E_n(t) &= E(0) + \frac{1}{\Gamma(\alpha)}\int_0^t (t-\rho)^{\alpha-1} K_2(\rho, E_{n-1}(\rho))d\rho,\\
Q_n(t) &= Q(0) + \frac{1}{\Gamma(\alpha)}\int_0^t (t-\rho)^{\alpha-1} K_3(\rho, Q_{n-1}(\rho))d\rho,\\
I_n(t) &= I(0) + \frac{1}{\Gamma(\alpha)}\int_0^t (t-\rho)^{\alpha-1} K_4(\rho, I_{n-1}(\rho))d\rho,\\
H_n(t) &= H(0) + \frac{1}{\Gamma(\alpha)}\int_0^t (t-\rho)^{\alpha-1} K_5(\rho, H_{n-1}(\rho))d\rho,\\
R_n(t) &= R(0) + \frac{1}{\Gamma(\alpha)}\int_0^t (t-\rho)^{\alpha-1} K_6(\rho, R_{n-1}(\rho))d\rho.
\end{aligned} \tag{14}
$$

The form presented below is the successive terms along the initial conditions of the model with their corresponding differences;

$$
\begin{aligned}
\Phi_{S,n}(t) &= S_n(t) - S_{n-1}(t) &&= \frac{1}{\Gamma(\alpha)}\int_0^t (t-\rho)^{\alpha-1}(K_1(\rho, S_{n-1}(\rho)) - K_1(\rho, S_{n-2}(\rho)))d\rho,\\
\Phi_{E,n}(t) &= E_n(t) - E_{n-1}(t) &&= \frac{1}{\Gamma(\alpha)}\int_0^t (t-\rho)^{\alpha-1}(K_2(\rho, E_{n-1}(\rho)) - K_2(\rho, E_{n-2}(\rho)))d\rho,\\
\Phi_{Q,n}(t) &= Q_n(t) - Q_{n-1}(t) &&= \frac{1}{\Gamma(\alpha)}\int_0^t (t-\rho)^{\alpha-1}(K_3(\rho, Q_{n-1}(\rho)) - K_3(\rho, Q_{n-2}(\rho)))d\rho,\\
\Phi_{I,n}(t) &= I_n(t) - I_{n-1}(t) &&= \frac{1}{\Gamma(\alpha)}\int_0^t (t-\rho)^{\alpha-1}(K_4(\rho, I_{n-1}(\rho)) - K_4(\rho, I_{n-1}(\rho)))d\rho,\\
\Phi_{H,n}(t) &= H_n(t) - H_{n-1}(t) &&= \frac{1}{\Gamma(\alpha)}\int_0^t (t-\rho)^{\alpha-1}(K_5(\rho, H_{n-1}(\rho)) - K_5(\rho, H_{n-2}(\rho)))d\rho,\\
\Phi_{R,n}(t) &= R_n(t) - R_{n-1}(t) &&= \frac{1}{\Gamma(\alpha)}\int_0^t (t-\rho)^{\alpha-1}(K_6(\rho, R_{n-1}(\rho)) - K_6(\rho, R_{n-2}(\rho)))d\rho.
\end{aligned} \tag{15}
$$

It is noticed that, $S_n(t) = \sum_{j=0}^{n} \Phi_{S,j}(t)$, $E_n(t) = \sum_{j=0}^{n} \Phi_{E,j}(t)$,$Q_n(t) = \sum_{j=0}^{n} \Phi_{Q,j}(t)$,$I_n(t) = \sum_{j=0}^{n} \Phi_{Q,j}(t)$,$I_n(t) = \sum_{j=0}^{n} \Phi_{I,j}(t)$,$H_n(t) = \sum_{j=0}^{n} \Phi_{H,j}(t)$,$R_n(t) = \sum_{j=0}^{n} \Phi_{R,j}(t)$. Now, we consider that:

$$\Phi_{S,n-1}(t) = S_{n-1}(t) - S_{n-2}(t), \Phi_{E,n-1}(t) = E_{n-1}(t) - E_{n-2}(t), \Phi_{Q,n-1}(t) = Q_{n-1}(t) - Q_{n-2}(t),$$

$$\Phi_{I,n-1}(t) = I_{n-1}(t) - I_{n-2}(t), \Phi_{H,n-1}(t) = H_{n-1}(t) - H_{n-2}(t), \Phi_{R,n-1}(t) = R_{n-1}(t) - R_{n-2}(t).$$

We obtained form (15),

$$
\begin{aligned}
\|\Phi_{S,n}(t)\| &\leq \frac{1}{\Gamma(\alpha)} g_1 \int_0^t (t-\rho)^{\alpha-1} \|\Phi_{S,n-1}(\rho)\| d\rho,\\
\|\Phi_{E,n}(t)\| &\leq \frac{1}{\Gamma(\alpha)} g_2 \int_0^t (t-\rho)^{\alpha-1} \|\Phi_{E,n-1}(\rho)\| d\rho,
\end{aligned} \tag{16}
$$

$$\|\Phi_{Q,n}(t)\| \leq \frac{1}{\Gamma(\alpha)} g_3 \int_0^t (t-\rho)^{\alpha-1} \|\Phi_{Q,n-1}(\rho)\| d\rho,$$
$$\|\Phi_{I,n}(t)\| \leq \frac{1}{\Gamma(\alpha)} g_4 \int_0^t (t-\rho)^{\alpha-1} \|\Phi_{I,n}(\rho)\| d\rho,$$
$$\|\Phi_{H,n}(t)\| \leq \frac{1}{\Gamma(\alpha)} g_5 \int_0^t (t-\rho)^{\alpha-1} \|\Phi_{H,n-1}(\rho)\| d\rho,$$
$$\|\Phi_{R,n}(t)\| \leq \frac{1}{\Gamma(\alpha)} g_6 \int_0^t (t-\rho)^{\alpha-1} \|\Phi_{R,n-1}(\rho)\| d\rho.$$

Hence, all the model variables depict the bounded functions and the representation of the kernels satisfies the Lipschitz condition. □

**Theorem 3**. *The Caputo COVID-19 model stated by system* (8) *has a unique solution for all value of t, such that* $t \in [0,a]$ *if*

$$\frac{1}{\Gamma(\alpha)} g_{jm} < 1, j = 1,...,6 \tag{17}$$

*Proof.* From the above theorem, one will notice that all the model variables depict the bounded functions and the expressions of the kernels satisfy the Lipschitz condition. Applying recursive principle on equation (17) with respect to system (8), the system below is obtained:

$$\|\Phi_{S,n}(t)\| \leq \|S_0(t)\| \left(\frac{m}{\Gamma(\alpha)} g_1\right)^n,$$
$$\|\Phi_{E,n}(t)\| \leq \|E_0(t)\| \left(\frac{m}{\Gamma(\alpha)} g_2\right)^n,$$
$$\|\Phi_{Q,n}(t)\| \leq \|Q_0(t)\| \left(\frac{m}{\Gamma(\alpha)} g_3\right)^n,$$
$$\|\Phi_{I,n}(t)\| \leq \|I_0(t)\| \left(\frac{m}{\Gamma(\alpha)} g_4\right)^n,$$
$$\|\Phi_{H,n}(t)\| \leq \|H_0(t)\| \left(\frac{m}{\Gamma(\alpha)} g_5\right)^n,$$
$$\|\Phi_{R,n}(t)\| \leq \|R_0(t)\| \left(\frac{m}{\Gamma(\alpha)} g_6\right)^n.$$

Hence, the progression exist and satisfy the conditions describes $\|\Phi_{S,n}(t)\| \longrightarrow 0$, $\|\Phi_{E,n}(t)\| \longrightarrow 0$,$\|\Phi_{Q,n}(t)\| \longrightarrow 0$,$\|\Phi_{I,n}(t)\| \longrightarrow 0$,$\|\Phi_{H,n}(t)\| \longrightarrow 0$, and $\|\Phi_{R,n}(t)\| \longrightarrow 0$, as $n \longrightarrow \infty$.

$$\|S_{n+1}(t) - S_n(t)\| \leq \sum_{n+1}^{j=n+1} Y_1^j \quad = \frac{Y_1^{n+1} - Y_1^{n+g+1}}{1-Y_1},$$

$$\begin{aligned}
\|E_{n+1}(t)-E_n(t)\| &\leq \sum_{n+1}^{j=n+1} Y_2^j = \frac{Y_1^{n+1}-Y_2^{n+g+1}}{1-Y_2},\\
\|Q_{n+1}(t)-Q_n(t)\| &\leq \sum_{n+1}^{j=n+1} Y_3^j = \frac{Y_1^{n+1}-Y_3^{n+g+1}}{1-Y_3},\\
\|I_{n+1}(t)-I_n(t)\| &\leq \sum_{n+1}^{j=n+1} Y_4^j = \frac{Y_1^{n+1}-Y_4^{n+g+1}}{1-Y_4},\\
\|H_{n+1}(t)-H_n(t)\| &\leq \sum_{n+1}^{j=n+1} Y_5^j = \frac{Y_1^{n+1}-Y_5^{n+g+1}}{1-Y_5},\\
\|R_{n+1}(t)-R_n(t)\| &\leq \sum_{n+1}^{j=n+1} Y_6^j = \frac{Y_1^{n+1}-Y_6^{n+g+1}}{1-Y_6}.
\end{aligned}$$

So by hypothesis, $\frac{1}{\Gamma(\alpha)} g_{jm} < 1$, and $S_n, E_n, Q_n, I_n, H_n, R_n$ is the Cauchy progression. By this, the complete desired result for the model (8) is obtained. □

**4.2. Iterative solution and stability analysis.** The subsequent hypothesis and solutions have been furnished to stabilize the outcome of this proposed model (8)

**Theorem 4** *Let ($\mathscr{B}$, $\|.\|$) indicate a Banach space, and $X^*$ defined a self map on $\mathscr{B}$. Further, $z_{n+1} = x(X^*, z_n)$ exhibits the recursive expression while $\mathscr{C}(X^*)$ implies the fixed point set upon $X^*$ indicating the fixed point set upon $X^*$. Also, by defining such that $\|y^*_{n+1} - x(X^*, y^*_n)\|$ such that $\{y^*_n \subseteq \mathscr{B}\}$. Then, in the iterative approach, $y_{n+1} = x(X^*, y_n), X^*$ is stable if $lim_{n\longrightarrow\infty} C_n = 0$, that is $lim_{n\longrightarrow\infty} C^*_n = p^*$ for $z_{n+1} = X^*$ where n is put up with as the Picard's iteration then $X^*$ iteration is stable. The hypothesis can be condensed as below. Let ($\mathscr{B}$, $\|.\|$) define a Banach space and $X^*$ be a self-map upon $\mathscr{B}$, then for all $x, y \in \mathscr{B}$, we have that*

$$\begin{aligned}
S_{n+1}(t) &= S_n(t) + \mathscr{L}^{-1}\left\{\frac{1}{S^a}\mathscr{L}\left\{\Lambda + \rho Q - \frac{\beta S(I+\varepsilon H)}{N} - \mu S - d_0 S\right\}\right\},\\
E_{n+1}(t) &= E_n(t) + \mathscr{L}^{-1}\left\{\frac{1}{S^a}\mathscr{L}\left\{\frac{\beta S(I+\varepsilon H)}{N} - (\delta+\psi+d_0)E\right\}\right\},\\
Q_{n+1}(t) &= Q_n(t) + \mathscr{L}^{-1}\left\{\frac{1}{S^a}\mathscr{L}\left\{\mu S + \delta E - (h_2+\rho+d_0)Q\right\}\right\},\\
I_{n+1}(t) &= I_n(t) + \mathscr{L}^{-1}\left\{\frac{1}{S^a}\mathscr{L}\left\{\psi E - (h_1+d_0+d_1)I\right\}\right\},\\
H_{n+1}(t) &= H_n(t) + \mathscr{L}^{-1}\left\{\frac{1}{S^a}\mathscr{L}\left\{h_1 I + h_2 Q - (\sigma(b,H)+d_0+d_1)H\right\}\right\},\\
R_{n+1}(t) &= R_n(t) + \mathscr{L}^{-1}\left\{\frac{1}{S^a}\mathscr{L}\left\{\sigma(b,H)H - d_0 R\right\}\right\}.
\end{aligned} \tag{18}$$

Suppose $\mathscr{Z}$ is defined as a self map, and the following results are obtained:

$$
\begin{aligned}
\mathscr{Z}[S_n(t)] &= S_{n+1}(t) &&= S_n(t) + \mathscr{L}^{-1}\left\{\frac{1}{S^a}\mathscr{L}\left\{\Lambda+\rho Q-\frac{\beta S(I+\varepsilon H)}{N}-\mu S-d_0 S\right\}\right\},\\
\mathscr{Z}[E_n(t)] &= E_{n+1}(t) &&= E_n(t) + \mathscr{L}^{-1}\left\{\frac{1}{S^a}\mathscr{L}\left\{\frac{\beta S(I+\varepsilon H)}{N}-(\delta+\psi+d_0)E\right\}\right\},\\
\mathscr{Z}[Q_n(t)] &= Q_{n+1}(t) &&= Q_n(t) + \mathscr{L}^{-1}\left\{\frac{1}{S^a}\mathscr{L}\{\mu S+\delta E-(h_2+\rho+d_0)Q\}\right\},\\
\mathscr{Z}[I_n(t)] &= I_{n+1}(t) &&= I_n(t) + \mathscr{L}^{-1}\left\{\frac{1}{S^a}\mathscr{L}\{\psi E-(h_1+d_0+d_1)I\}\right\},\\
\mathscr{Z}[H_n(t)] &= H_{n+1}(t) &&= H_n(t) + \mathscr{L}^{-1}\left\{\frac{1}{S^a}\mathscr{L}\{h_1 I+h_2 Q-(\sigma(b,H)+d_0+d_1)H\}\right\},\\
\mathscr{Z}[R_n(t)] &= R_{n+1}(t) &&= R_n(t) + \mathscr{L}^{-1}\left\{\frac{1}{S^a}\mathscr{L}\{\sigma(b,H)H-d_0 R\}\right\}.
\end{aligned}
\tag{19}
$$

$\mathscr{Z}$ is stable if the following conditions are satisfied

$\{1-\Lambda-\beta(Q_1+Q_2)f_1-\beta(Q_1+Q_2)f_2-T_0k_1\}<1$, $\{1-\beta(Q_1+Q_2)f_1+\beta(Q_1+Q_2)f_2-T_1k_2\}<1$,

$\{1-(\mu+\delta-(h_2+\rho+d_0))k_3\}<1$, $\{1-(\psi-(h_1+d_0+d_1))k_4\}<1$,

$\{1-(h_1+h_2-(\sigma+d_0+d_1))k_5\}<1$, $\{1-(\sigma-d_0)k_6\}<1$.

*Proof.* Let $T_0=\mu+d_0-\rho$ and $T_1=\delta+\psi+d_0$

The following equations were obtained when evaluated around the map $\mathscr{Z}$ which is a fixed point,

$$
\begin{aligned}
\mathscr{Z}[S_n(t)] - \mathscr{Z}[S_m(t)] &= S_n(t) - S_m(t),\\
\mathscr{Z}[E_n(t)] - \mathscr{Z}[E_m(t)] &= E_n(t) - E_m(t),\\
\mathscr{Z}[Q_n(t)] - \mathscr{Z}[Q_m(t)] &= Q_n(t) - Q_m(t),\\
\mathscr{Z}[I_n(t)] - \mathscr{Z}[I_m(t)] &= I_n(t) - I_m(t),\\
\mathscr{Z}[H_n(t)] - \mathscr{Z}[H_m(t)] &= H_n(t) - H_m(t),\\
\mathscr{Z}[R_n(t)] - \mathscr{Z}[R_m(t)] &= R_n(t) - R_m(t).
\end{aligned}
\tag{20}
$$

Taking the norm of both sides of the above equation

(21)

$$
\begin{aligned}
\| \mathscr{Z}[S_n(t)] - \mathscr{Z}[S_m(t)] \| &= \| \mathscr{L}^{-1}\left\{\frac{1}{S^a}\mathscr{L}\left\{\Lambda+\rho Q_n-\frac{\beta S_n(I_n+\varepsilon H_n)}{N}-\mu S_n-d_0 S_n\right\}\right\}\\
&\quad -\mathscr{L}^{-1}\left\{\frac{1}{S^a}\mathscr{L}\left\{\Lambda+\rho Q_m-\frac{\beta S_m(I_m+\varepsilon H_m)}{N}-\mu S_m-d_0 S_m\right\}\right\}\\
&\quad S_n(t)-S_m(t) \| .
\end{aligned}
$$

Further simplification of (21), leads;

$$\begin{aligned} \| \mathscr{Z}[S_n(t)] - \mathscr{Z}[S_m(t)] \| \quad &\leq \| S_n(t) - S_m(t) \| + \mathscr{L}^{-1}\{\frac{1}{S^a}\mathscr{L}\{\| \rho(Q_n - Q_m) \| \\ &+ \| \beta S_n(I_n - I_m) \| + \| \beta S_n \varepsilon (H_n - H_m) \| \frac{1}{N} \\ &- \| \mu(S_n - S_m) \| - \| d_0(S_n - S_m) \|\}\}. \end{aligned} \tag{22}$$

Using these assumptions,

$$\begin{aligned} \| E_n(t) - E_m(t) \| &\cong \| S_n(t) - S_m(t) \|, \\ \| Q_n(t) - Q_m(t) \| &\cong \| S_n(t) - S_m(t) \|, \\ \| I_n(t) - I_m(t) \| &\cong \| S_n(t) - S_m(t) \|, \\ \| H_n(t) - H_m(t) \| &\cong \| S_n(t) - S_m(t) \|, \\ \| R_n(t) - R_m(t) \| &\cong \| S_n(t) - S_m(t) \|, \end{aligned} \tag{23}$$

after putting the above relation, leads

$$\begin{aligned} \| \mathscr{Z}[S_n(t)] - \mathscr{Z}[S_m(t)] \| \quad &\leq \| S_n(t) - S_m(t) \| + \mathscr{L}^{-1}\{\frac{1}{S^a}\mathscr{L}\{\| \rho(Q_n - Q_m) \| \\ &+ \| \beta S_n(I_n - I_m) \| + \| \beta S_n \varepsilon (H_n - H_m) \| \frac{1}{N} \\ &- \| \mu(S_n - S_m) \| - \| d_0(S_n - S_m) \|\}\}. \end{aligned} \tag{24}$$

Since the progressions $S_n(t),\ E_m(t),\ Q_m(t),\ I_m(t),\ H_m(t),\ R_m(t)$ are convergent and bounded, their exist six different constant $S_1 > 0,\ S_2 > 0,\ S_3 > 0,\ S_4 > 0,\ S_5 > 0$ and $S_6 > 0$ for all $t$. Then $\| S_n(t) \| < \| S_1 \|,\ \| E_m(t) \| < \| S_2 \|,\ \| Q_m(t) \| < \| S_3 \|,\ \| I_m(t) \| < \| S_4 \|,\ \| H_m(t) \| < \| S_5 \|,\ \| R_n(t) \| < \| S_6 \|,\ (m,n) \in \mathbb{N} \times \mathbb{N}$. Through the relation, we can attain

(25)

$$\begin{aligned} \| \mathscr{Z}[S_n(t)] - \mathscr{Z}[S_m(t)] \| &\leq \{1 - \Lambda - \beta(Q_1 + Q_2)f_1 - \beta(Q_1 + Q_2)f_2 - (\mu + d_0 - \rho)k_1\} \\ &\quad \| S_n(t) - S_m(t) \|, \\ \| \mathscr{Z}[E_n(t)] - \mathscr{Z}[E_m(t)] \| &\leq \{1 - \beta(Q_1 + Q_2)f_1 + \beta(Q_1 + Q_2)f_2 - (\delta + \psi + d_0)k_2\} \\ &\quad \| E_n(t) - E_m(t) \|, \\ \| \mathscr{Z}[Q_n(t)] - \mathscr{Z}[Q_m(t)] \| &\leq \{1 - (\mu + \delta - (h_2 + \rho + d_0))k_3\} \| Q_n(t) - Q_m(t) \|, \\ \| \mathscr{Z}[I_n(t)] - \mathscr{Z}[I_m(t)] \| &\leq \{1 - (\psi - (h_1 + d_0 + d_1))k_4\} \| I_n(t) - I_m(t) \|, \\ \| \mathscr{Z}[H_n(t)] - \mathscr{Z}[H_m(t)] \| &\leq \{1 - (h_1 + h_2 - (\sigma + d_0 + d_1))k_5\} \| H_n(t) - H_m(t) \|, \\ \| \mathscr{Z}P[R_n(t)] - \mathscr{Z}[R_m(t)] \| &\leq \{1 - (\sigma - d_0)k_6\} \| R_n(t) - R_m(t) \| . \end{aligned}$$

Hence, the proof is complete. □

**4.3. Disease-free equilibrium.** The fractional model has a disease-free equilibrium presented by

$$\mathbb{D}_0 = (S^0, E^0, Q^0, I^0, H^0, R^0) = \left(\frac{\Lambda}{d_0}, 0, 0, 0, 0, 0\right), \tag{26}$$

an event portraying a society free of infection. The basic reproduction number, $\mathscr{R}_0$, inferred as the anticipated number of secondary instances produced by a sole contagious person in a totally susceptible community throughout its contagious time is a boundary variable that enables us to foresee if the infection will stop or prevail [38]. Typically, $\mathscr{R}_0 < 1$ implies that the disease (COVID-19) cannot overrun the community, $\mathscr{R}_0 > 1$ implies that each affected person develops more than one secondary infected person, and $\mathscr{R}_0 = 1$ respects additional scrutiny. The resolution of $\mathscr{R}_0$ is performed utilizing the next-generation matrix method [38, 39]. Utilizing this procedure, we retain

$$F = \begin{pmatrix} 0 & 0 & \beta & \beta\varepsilon \\ 0 & 0 & 0 & 0 \\ 0 & 0 & 0 & 0 \\ 0 & 0 & 0 & 0 \end{pmatrix} \tag{27}$$

and

$$V = \begin{pmatrix} k_2 & 0 & 0 & 0 \\ -\delta & k_3 & 0 & 0 \\ -\psi & 0 & k_4 & 0 \\ 0 & -h_2 & -h_1 & k_5 \end{pmatrix}, \tag{28}$$

where $k_2 = (\delta + \psi + d_0)$, $k_3 = (h_2 + \rho + d_0)$, $k_4 = (h_1 + d_0 + d_1)$ and $k_5 = (\sigma_1 + d_0 + d_1)$. At the disease-free equilibrium, $\mathbb{D}_0$, $\sigma(b,H) = \sigma_1$. Thus, the $\mathscr{R}_0$ of model (8) is given by

$$\mathscr{R}_0 = \frac{\beta(\psi k_3 k_5 + \varepsilon(k_3\psi h_1 + k_4\delta h_2))}{k_2 k_3 k_4 k_5} = \frac{\beta\psi}{k_2 k_4} + \frac{\beta\varepsilon(k_3\psi h_1 + k_4\delta h_2)}{k_2 k_3 k_4 k_5}. \tag{29}$$

The COVID-19 disease can be eradicated from the population ($\mathscr{R}_0 < 1$) if the initial sizes of the population of the model are in the basin of attraction of the disease-free equilibrium. This will be established by the following theorem.

**Theorem 5** *For any two positive integers $n_1^*, n_2^*$ with $gcd(n_1^*, n_2^*) = 1$ where $\alpha = \dfrac{n_1^*}{n_2^*}$ and $M = n_2^*$.*

*Thus, the system* (8) *is locally asymptotically stable if* $|\ arg(\lambda)\ | > \dfrac{\pi}{2M}$ *for every root of* $\lambda$ *that is represented by the following equation,*

$$det(diag[\lambda^{Ma}\lambda^{Ma}\lambda^{Ma}\lambda^{Ma}\lambda^{Ma}\lambda^{Ma}] - J(D_0)) = 0 \tag{30}$$

*Proof.* The Jacobian of system (8) at $D_0$ is

$$J(D_0) = \begin{pmatrix} -d_0 & 0 & \rho & -\beta & -\beta\varepsilon & 0 \\ 0 & -k_2 & 0 & \beta & \beta\varepsilon & 0 \\ 0 & \delta & -k_3 & 0 & 0 & 0 \\ 0 & \psi & 0 & -k_4 & 0 & 0 \\ 0 & 0 & h_2 & h_1 & -k_5 & 0 \\ 0 & 0 & 0 & 0 & \sigma_1 & -d_0 \end{pmatrix}, \tag{31}$$

The characteristics equation (31)

$$(\lambda^m + d_0)^2(\lambda^{4m} + a_1\lambda^{3m} + a_2\lambda^{2m} + a_3\lambda^m + a_4) = 0. \tag{32}$$

The replicated two eigenvalues are $-d_0, -d_0$, have a negative real part. We employ the polynomial in (32) and estimated the residing eigenvalues by finding the coefficients provided below:

$$\begin{aligned} a_1 &= k_2 + k_3 + k_4 + k_5, \\ a_2 &= k_2(k_3 + k_4 + k_5) + k_3(k_4 + k_5) + k_4k_5 - \psi\beta, \\ a_3 &= (k_2k_4 - \psi\beta)(k_3 + k_5) + k_3k_5(k_2 + k_3) - \beta\varepsilon(h_1\psi + h_2\delta), \\ a_4 &= k_2k_3k_4k_5(1 - \mathscr{R}_0). \end{aligned}$$

Obviously, $a_i$ are all positive for $i = 1, ..., 4$ if $\mathscr{R}_0 < 1$. The Routh-Hurtwiz criteria can be utilized to fulfill the conditions to prove the locally asymptotically stable of the system (8). This calculation can be performed easily through software computation. The argument of the roots of equation $(\lambda^m + d_0)^2 = 0$ are

$$arg(\lambda_k) = \frac{\pi}{m} + k\frac{2\pi}{m} > \frac{\pi}{M} + \frac{\pi}{2M}, where\ k = 0, 1, 2, ..., (m-1).$$

Similar calculation can be applied to show that the argument of the roots of Eq. (32) are all greater than $\dfrac{\pi}{2M}$ if $\mathscr{R}_0 < 1$. Moreover, we can determine an argument less than $\dfrac{\pi}{2M}$ for $\mathscr{R}_0 > 1$. Thus disease-free equilibrium is locally asymptotically stable for $\mathscr{R}_0 < 1$. □

**Lemma 1** *The disease-free equilibrium $\mathscr{D}_0$ is locally asymptotically stable whenever $\mathscr{R}_0 < 1$ and is unstable if $\mathscr{R}_0 > 1$.*

The epidemiological significance of Lemma (4.3) is that it is possible to curb COVID-19 (or alumina it) from a community (when $\mathscr{R}_0 < 1$) if the preliminary quantities of the sub-populations of the fractional model are in the bay of interest of the disease-free equilibrium ($\mathbb{D}_0$).

**4.4. Global stability of disease-free equilibrium.** To guarantee active management (or elimination) of COVID-19 in a community when it is autonomous of the preliminary quantity of the sub-populations of the fractional model (8), it is crucial to exhibit that the $\mathbb{D}_0$ is globally asymptotically stable (GAS). This will be performed by assigning the Lyapunov function procedure.

**Theorem 6** *The disease-free equilibrium ($\mathbb{D}_0$) of the fractional model* (8)*, given by* (26)*, in the shortage of the progression rate of people in class S to class Q ($\mu = 0$) is GAS if $\mathscr{R}_0 \leq 1$.*

*Proof.* Assess the fractional model (8) with $\mu = 0$ and the subsequent Lyapunov functional defined by

$$V = E + A_1 Q + A_2 I + A_3 H \tag{33}$$

Relating the Caputo-fractional derivative on $V$, concurrently with the practice of the model (8), we obtain,

$$^{C}D_t^{\alpha}\, V = {}^{C}D_t^{\alpha}\, E + A_1\, {}^{C}D_t^{\alpha}\, Q + A_2\, {}^{C}D_t^{\alpha}\, I + A_3\, {}^{C}D_t^{\alpha}\, H \tag{34}$$

where $A_1 = \dfrac{d_0}{\delta} - \dfrac{d_0 k_3 h_1 \psi}{(k_4\delta h_2 - \psi k_3 h_1)\delta}$, $A_2 = \dfrac{d_0 k_3 h_1}{k_4\delta h_2 - \psi k_3 h_1}$ and $A_3 = \dfrac{d_0 k_3}{\delta h_2} - \dfrac{d_0 k_3^2 h_1 \psi}{(k_4\delta h_2 - \psi k_3 h_1)\delta h_2}$.
The time derivative of the Lyapunov function (34), which is represented by $^{C}D_t^{\alpha}\, V^{'}$, along the solution path of system (8) with $\mu = 0$, is given by

$$\begin{aligned} {}^{C}D_t^{\alpha}\, V' = {} & \frac{\beta S(I+\varepsilon H)}{N} - d_0 E + \left[\frac{d_0}{\delta} - \frac{d_0 k_3 h_1 \psi}{(k_4\delta h_2 - \psi k_3 h_1)\delta}\right](\delta E - k_3 Q) \\ & + \left[\frac{d_0 k_3 h_1}{k_4\delta h_2 - \psi k_3 h_1}\right](\psi E - k_4 I) + \left[\frac{d_0 k_3}{\delta h_2} - \frac{d_0 k_3^2 h_1 \psi}{(k_4\delta h_2 - \psi k_3 h_1)\delta h_2}\right](h_1 I + h_2 Q - k_5 H) \end{aligned} \tag{35}$$

Using the limiting value $N = \dfrac{\Lambda}{d_0}$ and since $S \leq \dfrac{\Lambda}{d_0}$ in the positively-invariant region $\Phi$, it follows, by serious rigorous simplification of (35), results into

$$^{C}D_{t}^{\alpha}\, V' \leq \beta \left[\frac{\psi k_3 k_5 + \varepsilon(h_1\psi k_3 + h_2\delta k_4)}{\psi k_3 k_5}\right] I + \frac{d_0 k_3 h_1}{\delta h_2} - \frac{d_0(h_1\psi k_3 + h_2\delta k_4)}{\psi\delta h_2} I, \tag{36}$$

which finally yields this

$$^{C}D_{t}^{\alpha}\, V' \leq \beta \left[\frac{\psi k_3 k_5 + \varepsilon(h_1\psi k_3 + h_2\delta k_4)}{\psi k_3 k_5} - \frac{d_0 k_4}{\psi}\right] I \tag{37}$$

then,

$$^{C}D_{t}^{\alpha}\, V' \leq \frac{d_0 k_4}{\psi}(\mathscr{R}_0 - 1) I. \tag{38}$$

Hence $^{C}D_{t}^{\alpha}\, V \leq 0$, if $\mathscr{R}_0 < 1$. $^{C}D_{t}^{\alpha}\, V = 0$ if and only if $E = Q = I = H = 0$. Thus $(E,Q,I,H) \longrightarrow (0,0,0,0)$ as $t \longrightarrow \infty$ and model (8) implies that $S \longrightarrow \dfrac{\Lambda}{d_0}$ and $R \longrightarrow 0$ as $t \longrightarrow \infty$. It can be followed from the results given in [36], the solution of system (8) with non-negative initial conditions tends to $\mathbb{D}_0$ whenever $t \longrightarrow \infty$ in $\Phi$. So, the system (8) at $\mathbb{D}_0$ is globally asymptotically stable (GAS). □

**4.5. Endemic equilibrium.** The rate of change of the total population of the system (8) is given as

$$\frac{dN(t)}{dt} = \Lambda - \mu N(t), \tag{39}$$

so that, $N(t) \longrightarrow \dfrac{\Lambda}{\mu}$ as $t \longrightarrow \infty$. On the other hands, if $N^{**}$ is the value of the total population at equilibrium, then solving (39) at equilibrium point gives $N^{**} = \dfrac{\Lambda}{\mu}$. For convenience, let an endemic equilibrium of the fractional model (8) be denoted as

$$\mathscr{E}^{**} = (S^{**},\, E^{**},\, Q^{**},\, I^{**},\, H^{**},\, R^{**}) \tag{40}$$

Similarly, using $N^{**} = \dfrac{\Lambda}{\mu}$ at equilibrium, let the force of infection by

$$\lambda^{**} = \frac{\beta(I^{**} + \varepsilon H^{**})\mu}{\Lambda}. \tag{41}$$

Therefore, solving the system (8) at equilibrium is given by

(42)
$$S^{**} = \frac{\Lambda}{\lambda^{**} + d_0},\ E^{**} = \frac{\lambda^{**}\Lambda}{(\lambda^{**} + d_0)k_2},\ Q^{**} = \frac{\delta\lambda^{**}\Lambda}{(\lambda^{**} + d_0)k_2k_3}$$

$$I^{**} = \frac{\psi\lambda^{**}\Lambda}{(\lambda^{**} + d_0)k_2k_4},\ H^{**} = \frac{(h_1k_3\psi + h_2k_4\delta)\lambda^{**}\Lambda}{(\lambda^{**} + d_0)k_2k_3k_4k_5},\ R^{**} = \frac{\sigma_1\lambda^{**}\Lambda(h_1k_3\psi + h_2k_4\delta)}{d_0((\lambda^{**} + d_0)k_2k_3k_4k_5)}.$$

Substituting (42) into (41), and after simplification, we get

(43)
$$A_4\lambda^{**} + A_5 = 0,$$

where

(44)
$$A_4 = k_2k_3k_4k_5$$
$$A_5 = k_2k_3k_4k_5d_0(1 - \mathscr{R}_0).$$

If $\mathscr{R}_0 > 1$, then a unique endemic equilibrium exist.

**Lemma 2** *The system* (8) *has a unique endemic equilibrium ($\mathscr{E}^{**}$), whenever $\mathscr{R}_0 > 1$.*

The qualitative behavior of solutions with respect to Theorem (4.4) has shown in Fig (2(a)) where solutions at different initial conditions tends to the disease-free equilibrium point asymptotically. This result implies that the disease elimination is possible regardless of the number of infectious individuals present in the population as long as the basic reproduction number of the disease is less than unity. Similarly, Fig (2(b)) shows the population of infected individuals at different initial conditions converge to endemic equilibrium point when the basic reproduction number is greater than unity. The implication is that the disease will persist in the population regardless of the number of infected individuals in the populations as long as the basic reproduction number of the disease is greater than unity.

**4.6. Sensitivity analysis.** In this section, the sensitivity analysis of the formulated model (6) is studied. In other to achieve this, the method used in the following literature [11, 19, 21, 36] were adopt. The purpose of this is to know the parameters of the model that contribute majorly to the spread of COVID-19 in the population. Thus, to do this the COVID-19 threshold quantity, the basic reproduction number $\mathscr{R}_0$ given in (29), as the response function with respect to the model parameters (6), the normalized forward-sensitivity index of $\mathscr{R}_0$ that depends on a parameter $p$ is defined as

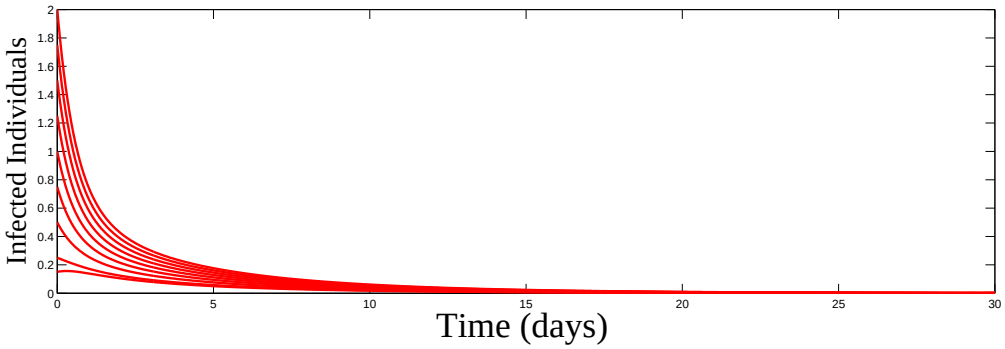


(A) Global asymptotic convergence of the model solution at different initial conditions to disease-free equilibrium when $\mathscr{R}_0 = 0.5417 < 1$. The parameter values used are presented in Table (3), except $\beta = 0.1321$ and $h_2 = 0.1002$

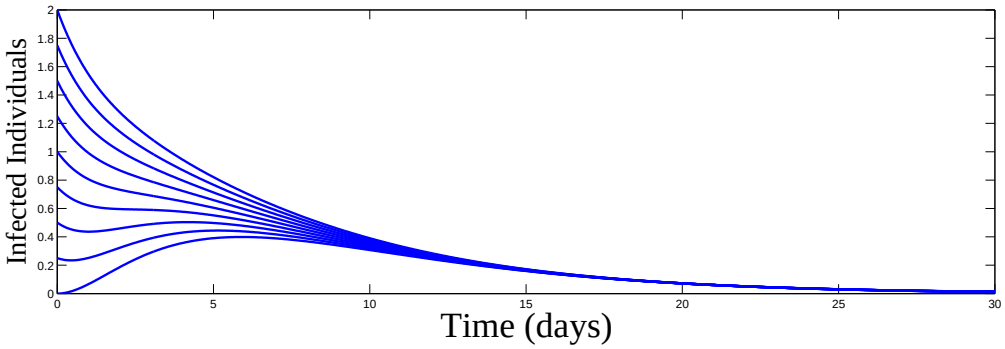


(B) Global asymptotic convergence of the model solution at different initial conditions to endemic equilibrium when $\mathscr{R}_0 = 1.4592 > 1$. The parameter values used are presented in Table (3)

FIGURE 2. Simulation of the global asymptotic convergence of the system (6) solution at different initial conditions

$$\Upsilon_p^{\mathscr{R}_0} = \frac{\partial \mathscr{R}_0}{\partial p} \times \frac{p}{\mathscr{R}_0}. \tag{45}$$

Given the explicit formula (29) for the basic reproduction number $\mathscr{R}_0$, the analytical expressions for the sensitivity of $\mathscr{R}_0$ in respect of the parameters defining it are computed. In particular, the analytical expression for the sensitivity of $\mathscr{R}_0$ with respect to $\beta$ in view of (45) is a constant value, while that of $\varepsilon$ is a complex expression, and are both obtained as

$$\Upsilon_\beta^{\mathscr{R}_0} = \frac{\partial \mathscr{R}_0}{\partial \beta} \times \frac{\beta}{\mathscr{R}_0} = +1.$$

In a similar manner, the analytical sensitivity indices of $\mathscr{R}_0$ for the other parameters are computed. But the results are omitted due to their complexity. However, the sensitivity index (SI) of $\mathscr{R}_0$ for all the parameters comprising it are evaluated at the baseline parameter values given in Table 3. The signs and values of SI are presented in Table 2.

TABLE 2. Sensitivity index of $\mathscr{R}_0$ to each of the parameters of model (6) evaluated at the baseline parameter values given in Table 3

| Parameter | Sign of SI |
|---|---|
| $\psi$ | *Positive* |
| $\varepsilon$ | *Positive* |
| $\delta$ | *Negative* |
| $h_1$ | *Negative* |
| $h_2$ | *Positive* |
| $d_0$ | *Negative* |
| $\rho$ | *Negative* |
| $\sigma_1$ | *Negative* |
| $d_1$ | *Negative* |
| $\beta$ | *Positive* |

From Table 2, it is observed that the sign of SI is positive for some parameters $(\psi, \varepsilon, h_2, \beta)$, while it is negative for the others $(\delta, h_1, d_0, \rho, \sigma_1, d_1)$. From the set of parameters with positive SI sign, $\beta$, $\varepsilon$ and $\psi$ are most positive. Whereas, $\sigma_1$, $\delta$ and $h_1$ are most negative from the set of parameters with negative SI signs. The epidemiological insight from the positive sign of SI of the COVID-19 threshold quantity, $\mathscr{R}_0$, is that increasing or decreasing the value of any of the parameters in this category will generate an increase or decrease in the threshold $\mathscr{R}_0$ of COVID-19. The negative sign of SI on the contrary suggests that increasing the value of each of the parameter set in this category will lead to a decrease in the $\mathscr{R}_0$ value, and vice-versa. For example, $S_{\beta}^{\mathscr{R}_0} = +1$ indicates that increasing the effective transmission rate of COVID-19 by 10% will increase the basic reproduction number, $\mathscr{R}_0$, of the disease by 10%, and the other way round. Similarly, $S_{\sigma_1}^{\mathscr{R}_0} \approx -0.44$ means that increasing (or decreasing) $\sigma_1$ by 100% always

decreases (or increases) $\mathscr{R}_0$ by 44%. Consequently, in view of the results of sensitivity analysis in Table 2, considerations of any control strategies that reduce the effective transmission rate of COVID-19 ($\beta$), modification parameter relative to the infectiousness of hospitalized ($\varepsilon$), progression rate from exposed to become symptomatic ($\psi$), and increase the maxima per capital recovery rate associated with the sufficient healthcare resources and few hospitalized humans ($\sigma_1$), detection rate for exposed self-quarantine ($\delta$) and hospitalization rate for symptomatic infectious ($h_1$) are needed to ensure an effective control of COVID-19 transmission and spread in the population. The Fig 3 below is the sensitivity value of COVID-19 model parameters.

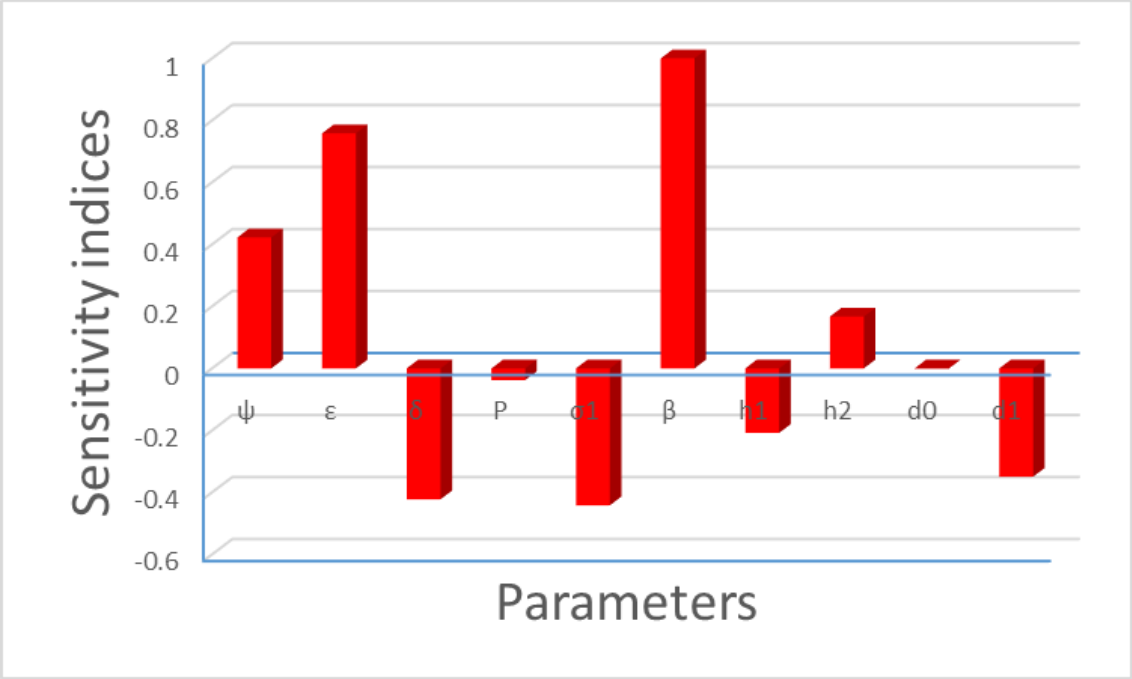


FIGURE 3. Sensitivity of COVID-19 model parameters

## 5. NUMERICAL SIMULATIONS AND DISCUSSION

The simulation for the Caputo COVID-19 model (8) is presented in this segment. The natural variable's significance for the numerical simulation is provided in Table 3. The proposed fractional model is unraveled numerically employing the notion explained in detail in [40, 41].

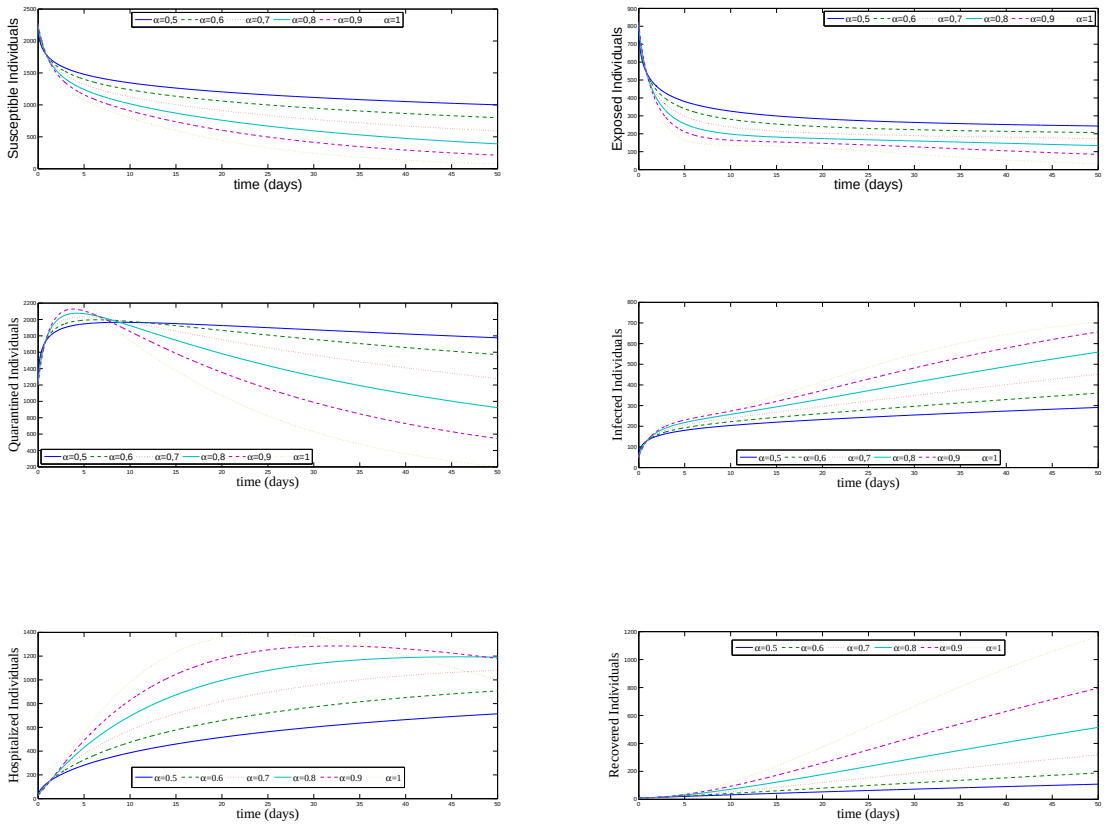


FIGURE 4. Simulation of the system (8) for various values of $\alpha$.

To review the position of numerous variables and memory inventories in the feature of the disease incidence, there have been many uses of the main variables of the model. The changing features of the proposed COVID-19 model (8) are exemplified graphically putting into account of time unit has days. The model's initial limitations are seized as

$$(S(0),E(0),Q(0),I(0),H(0),R(0)) = (2269,820,1200,50,27,9),$$

while the model variable values and their references are interpreted in Table 3.

TABLE 3. Variable values used in simulating model (8)

| Parameter | Value | Source | | Parameter | Value | Source |
|---|---|---|---|---|---|---|
| $\Lambda$ | 0.2266 | Assumed | | $\rho$ | 0.1945 | [11] |
| $\varepsilon$ | 0.24278 | [19] | | $\mu$ | 0.3938 | [11] |
| $d_0$ | $\frac{1}{60.45\times 365}$ | Assumed | | $\beta$ | 0.38974 | [19] |
| $\delta$ | 0.335 | Assumed | | $d_1$ | 0.015 | [19] |
| $\psi$ | $1/5.2$ | [19] | | $\alpha_0$ | 0.2 | [42] |
| $h_2$ | 0.2351 | Assumed | | $\sigma_1$ | 0.021 | Assumed |

Below we give the graphs obtained from the numerical simulation of our Caputo model.

In Fig.(4), several values of $\alpha$ have been examined on the model compartments graphically. The findings demonstrate that as the order of Caputo operator $\alpha$ rises, the burden of the syndrome rises in the community while the value $\alpha$ declines, and the different compartments are declines with time. The consequence of Effective transmission rate $\beta$ on the dynamics of the model is exemplified in Figure (5). This behavior is interpreted for two values of the order of Caputo operator i.e., $\alpha = 0.50, 0.90$. It was observed in Figure (5(a)) that as the effective transmission rate increases the exposed individual also increases as the day goes by when $\alpha = 0.5$, while in Figure (5(b)) as the effective transmission rate increases the exposed individual also increases for the first 27 days but convergence at the end of the day when $\alpha = 0.5$. On the other hand, in Figure 5(c) the effective transmission rate increases the quarantined individual decreases and convergence to endemic at the end when $\alpha = 0.5$ and in Figure 5(d) has the effective transmission rate increases the quarantined individual decreases and convergence to disease-free at the end (50 days) when $\alpha = 0.5$. In Figure 5(e) the effective transmission rate increases the infected individual also increases slowly as the day goes by when $\alpha = 0.5$, but in Figure 5(f) infected individuals increase greatly within this period when $\alpha = 0.5$. In Figure 5(g) the effective transmission rate decreases the hospitalized individual increase when $\alpha = 0.5$ and in Figure 5(h) as the effective transmission rate decreases the hospitalized individual increase and convergence to endemic at the end (50 days) when $\alpha = 0.9$.

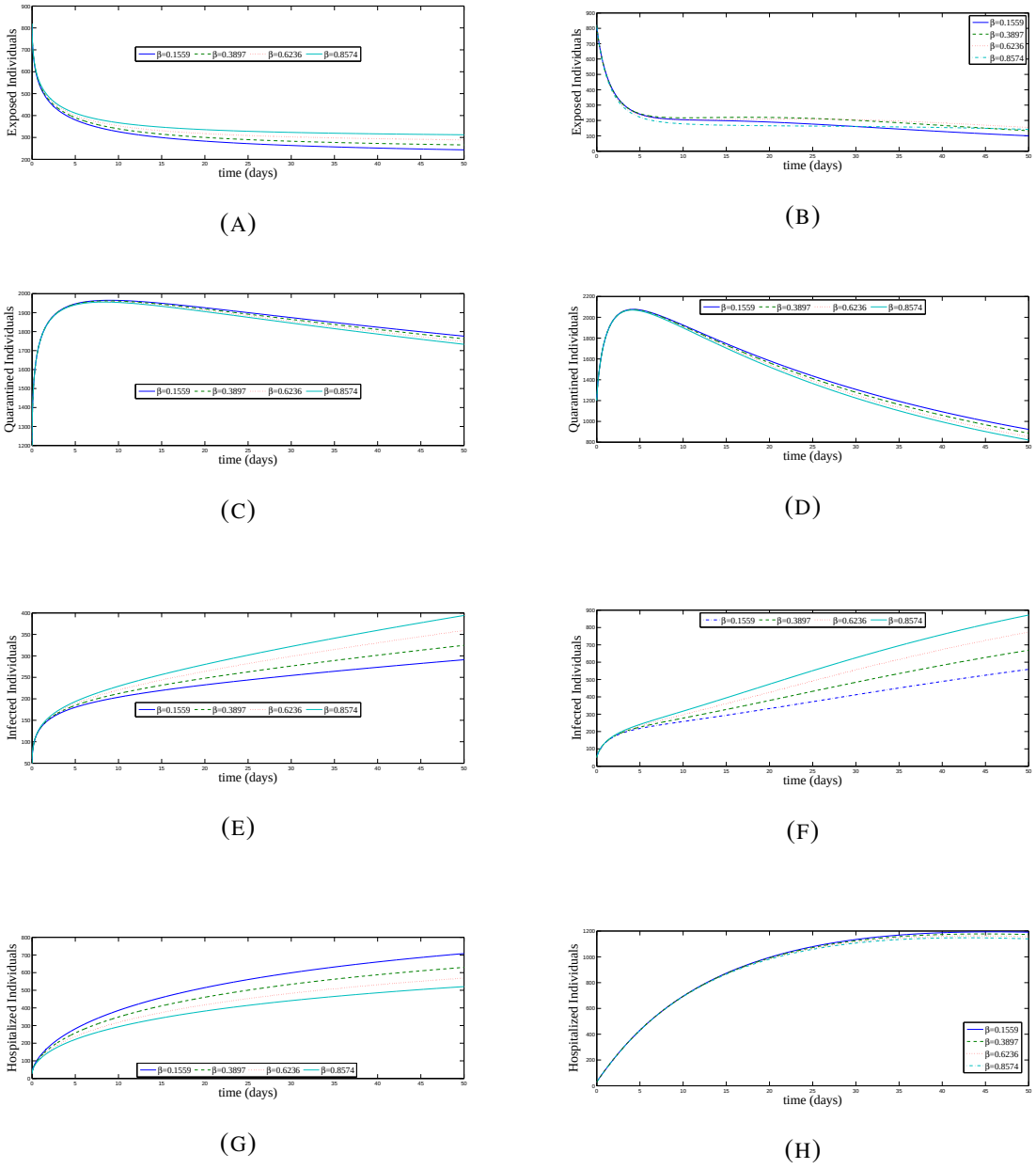


FIGURE 5. Simulation showing the effect of the transmission rate ($\beta$) on the population dynamics of COVID-19 for $\alpha = 0.5$ (a,c,e,g), $\alpha = 0.9$ (b,d,f,h).

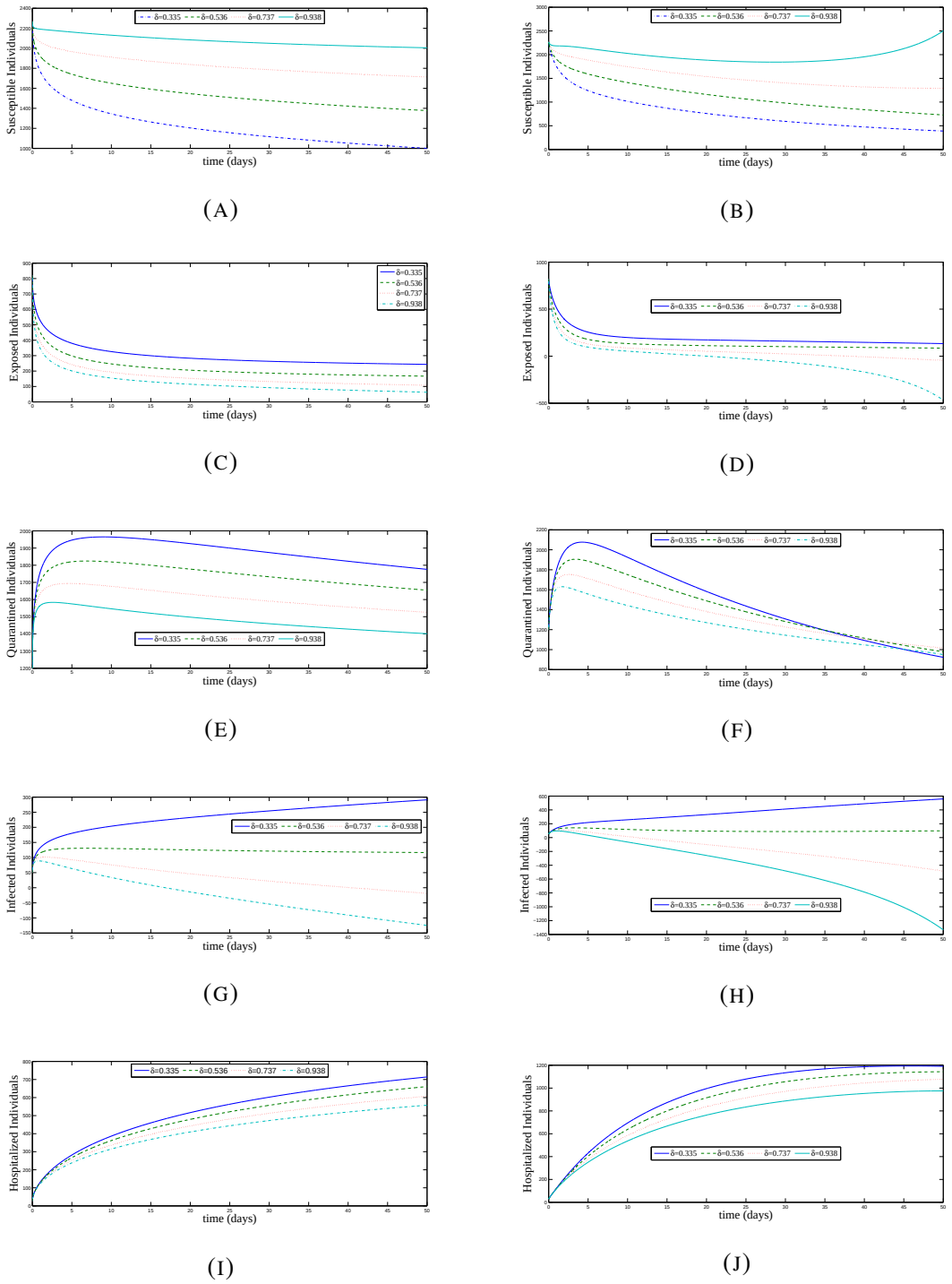


FIGURE 6. Simulation showing the effect of detection rate for exposed individuals to become quarantined ($\delta$) on the population dynamics of COVID-19 for $\alpha = 0.5$ (a,c,e,h,i), $\alpha = 0.9$ (b,d,f,h,j).

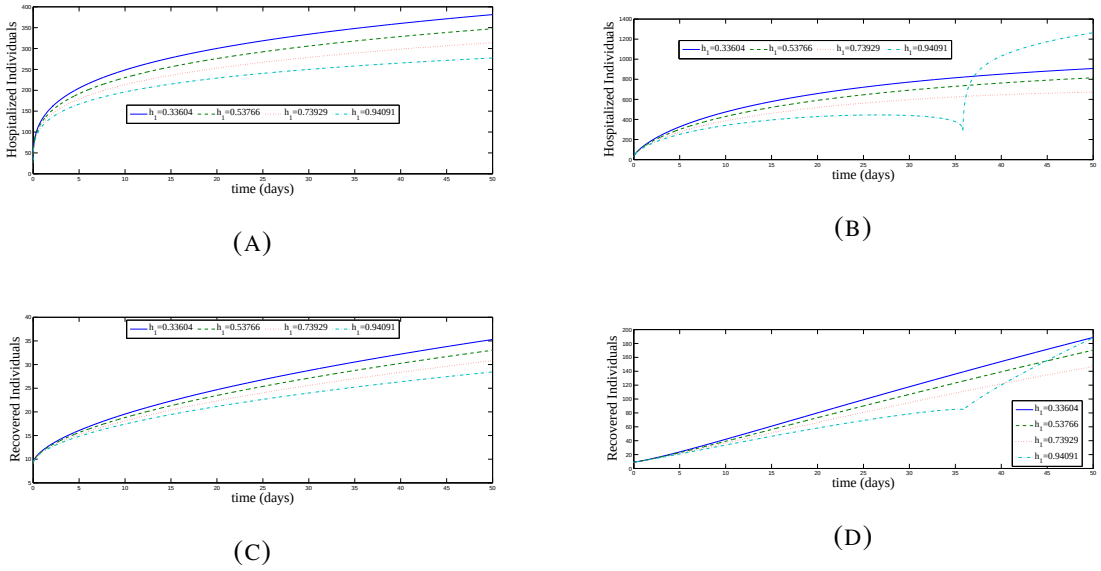


FIGURE 7. Simulation showing the effect of hospitalization rates for infectious ($h_1$) on the population dynamics of COVID-19 for $\alpha = 0.5$ (a,c), $\alpha = 0.9$ (b,d).

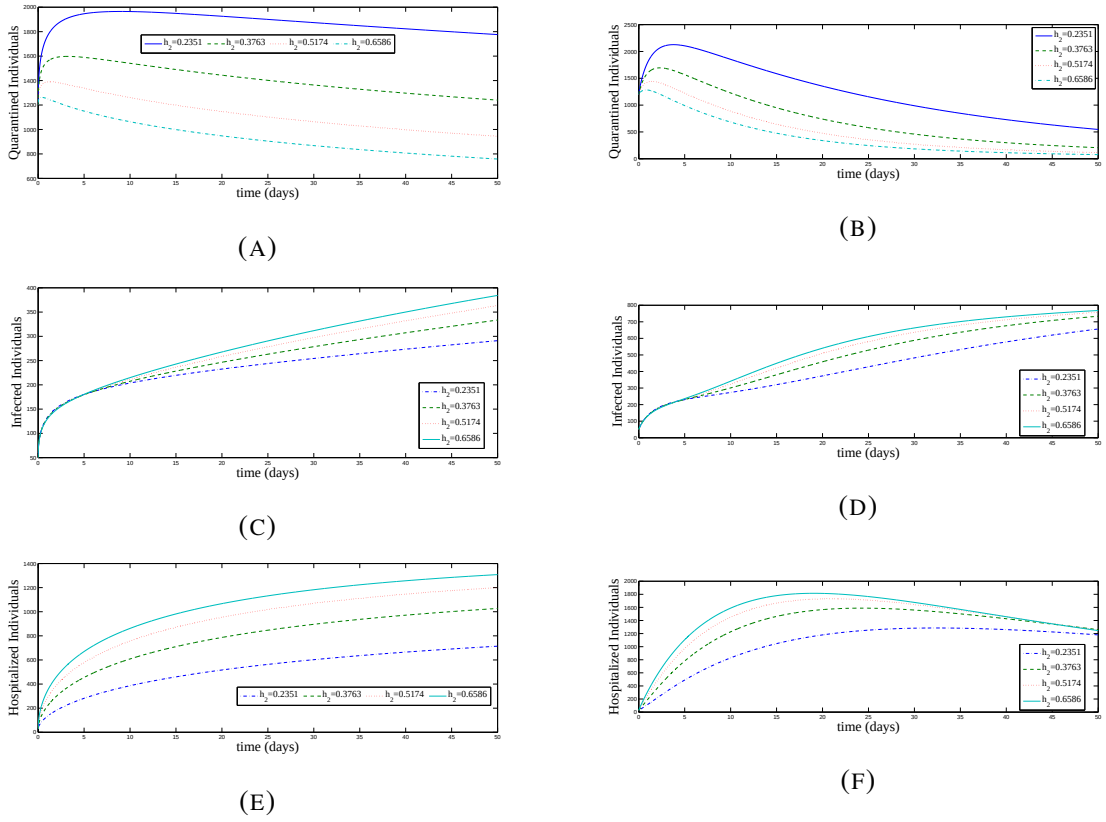


FIGURE 8. Simulation showing the effect of hospitalization rates for quarantined, ($h_2$) on the population dynamics of COVID-19 for $\alpha = 0.5$ (a,c,e,), $\alpha = 0.9$ (b,d,f).

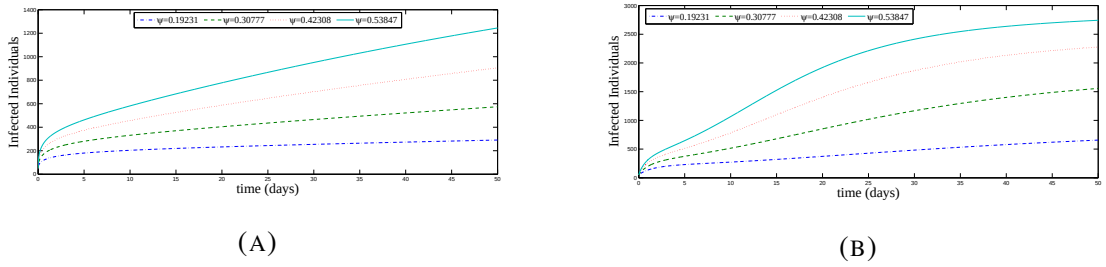


FIGURE 9. Simulation showing the effect of disease progression rate from exposed class ($\psi$) on the population dynamics of COVID-19 for $\alpha = 0.5$ (a), $\alpha = 0.9$ (b).

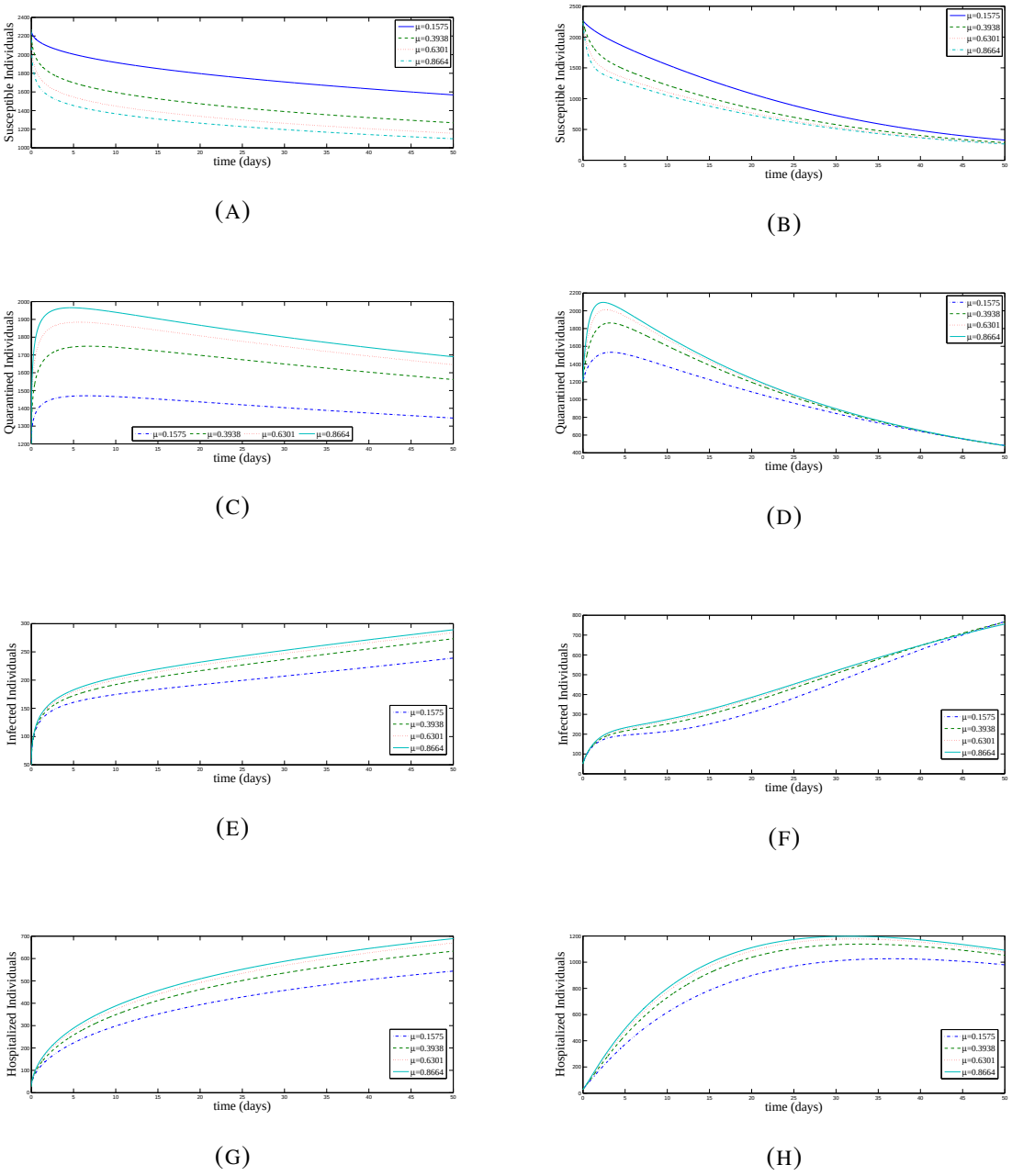


FIGURE 10. Simulation showing the effect of progression rate of individuals in class S to class Q ($\mu$) on the population dynamics of COVID-19 for $\alpha = 0.5$ (a,c,e,g), $\alpha = 0.9$ (b,d,f,h).

Also, Figure 6 shows the effect of the detection rate for exposed individuals to become quarantined $\delta$. In Figure 6(a)–6(b) the susceptible individual increases as the detection rate for exposed individuals to become quarantined increases, while in Figure 6(c)–6(d) the exposed individual increases as the detection rate for exposed individuals to become quarantined decrease. In Figure 6(e) the quarantined individual increases as the detection rate for exposed individuals to become quarantined decreases but in Figure 6(f) it convergence to endemic over time. In Figure 6(g)–6(h) the infected individual increases as the detection rate for exposed individuals to become quarantined decreases, while in Figure 6(i)–6(j) the hospitalized individual decreases as the detection rate for exposed individuals to become quarantined increase. The impact of hospitalized rates for infectious $h_1$ on the population dynamics of COVID-19 is depicted in Figure 7. By increasing the value of the hospitalized rate, one can observe the decrease in the hospitalized and recovered individuals when $\alpha = 0.5$ as shown in Figure 7(a)–7(c) but when $\alpha = 0.9$ similar things occur for the first 36 days, as h1 approaches its optimal, the hospitalized and recovered individuals increases sporadically as shown in Figure 7(b)–7(d). The impact of hospitalized rates for quarantined, $h_2$ on the dynamics of the model are illustrated in Figure 8. In Figure 8(a)–8(b) as the $h_2$ increases the quarantined individual also decreases with time, and in Figure 8(c)–8(d) as the $h_2$ increases the infected individual also increases with time and similarly to the hospitalized individual as shown in Figure 8(e)–8(f).

Similarly, Figure 9 shows the effect of disease progression rate from exposed class ($\psi$) on the population dynamics of COVID-19. In Figure 9(a)–9(b) as $\psi$ increases also infected community increased. In Figure 10 as the effect of progression rate of individuals in class S to class $Q$ increases quarantined, infected, and hospitalized class increase for both $\alpha$ with time but $\alpha = 0.9$ it convergence at a point for quarantined and infected class and reaches a peck at maximum for hospitalized class at 30 days.

## 6. CONCLUSION

In this paper, we formulate and analyze a Caputo fractional model of COVID-19 incorporating the potential impact of limited resources on the human population. Mathematical analyses of the model were done, which included determining the well-posedness of the system, equilibrium point, basic reproduction number $\mathscr{R}_0$ and the existence and uniqueness of solutions, as well as the global stabilities of the model equilibria, were established based on the $\mathscr{R}_0$. Our model basic reproduction number was calculated analytically and then evaluated numerically to be $\mathscr{R}_0 = 1.4592$ which indicates the high transmissibility of the COVID-19 virus in the population induced by the disease. Sensitivity analysis was also carried out to know the contributory effect of each parameter on the dynamical spread of COVID-19 in the community. Importantly, the qualitative analysis of the model shows that an increase in the fractional order parameter leads to an increase in the number of humans infected with COVID-19. Furthermore, in the absence of resources such as masks, limited hospital beds, and various other non-pharmaceutical interventions, our model predicts an increase in the number of infectious individuals as more people get exposed to the virus. Similarly, the results of this model will help policymakers to devise strategies to reduce the COVID-19 infection. We acknowledge that the modeling presented in this paper has a limitation; the model is not fitted to the COVID-19 epidemiological dataset for any specific region. Rather we parameterize our model using the available parameter values from published literature which conforms with the actual attributes of COVID-19 dynamics. The work presented in this manuscript can be extended by incorporating fractional optimal control parameters, which may investigate the types of interventions required to reduce COVID-19 viral transmission in an event for a population with inadequate resources.

### ACKNOWLEDGMENTS

The authors will like to acknowledge the respective universities for the production of this manuscript

### CONFLICT OF INTERESTS

The authors declare that there is no conflict of interests.

## REFERENCES


[1] N. Zhong, B. Zheng, Y. Li, et al. Epidemiology and cause of severe acute respiratory syndrome (SARS) in Guangdong, People's Republic of China, in February, 2003, The Lancet. 362 (2003), 1353–1358. https://doi.org/10.1016/s0140-6736(03)14630-2.

[2] J. Cao, X. Hu, W. Cheng, et al. Clinical features and short-term outcomes of 18 patients with corona virus disease 2019 in intensive care unit, Intensive Care Med. 46 (2020), 851–853. https://doi.org/10.1007/s00134-020-05987-7.

[3] J. Cao, W.J. Tu, W. Cheng, et al. Clinical features and short-term outcomes of 102 patients with coronavirus disease 2019 in Wuhan, China, Clinic. Infect. Dis. 71 (2020), 748–755. https://doi.org/10.1093/cid/ciaa243.

[4] C.J. Edholm, B. Levy, L. Spence, et al. A vaccination model for COVID-19 in Gauteng, South Africa, Infect. Dis. Model. 7 (2022), 333–345. https://doi.org/10.1016/j.idm.2022.06.002.

[5] World Health Organization (WHO). https://www.who.int/emergencies/diseases/novel-coronavirus-2019. Accessed in July 9, 2022.

[6] M. Farman, M. Aslam, A. Akgul, et al. Modeling of fractional-order COVID-19 epidemic model with quarantine and social distancing, Math. Meth. Appl. Sci. 44 (2021), 9334–9350. https://doi.org/10.1002/mma.7360.

[7] C.N. Ngonghala, E. Iboi, S. Eikenberry, et al. Mathematical assessment of the impact of non-pharmaceutical interventions on curtailing the 2019 novel Coronavirus, Math. Biosci. 325 (2020), 108364. https://doi.org/10.1016/j.mbs.2020.108364.

[8] K. Shah, T. Abdeljawad, I. Mahariq, et al. Qualitative analysis of a mathematical model in the time of COVID-19, BioMed Res. Int. 2020 (2020), 5098598. https://doi.org/10.1155/2020/5098598.

[9] K. Shah, Z.A. Khan, A. Ali, et al. Haar wavelet collocation approach for the solution of fractional order COVID-19 model using Caputo derivative, Alexandria Eng. J. 59 (2020), 3221–3231. https://doi.org/10.1016/j.aej.2020.08.028.

[10] S.S. Musa, S. Zhao, M.H. Wang, et al. Estimation of exponential growth rate and basic reproduction number of the coronavirus disease 2019 (COVID-19) in Africa, Infect. Dis. Poverty. 9 (2020), 96. https://doi.org/10.1186/s40249-020-00718-y.

[11] A. Abidemi, Z.M. Zainuddin, N.A.B. Aziz, Impact of control interventions on COVID-19 population dynamics in Malaysia: a mathematical study, Eur. Phys. J. Plus. 136 (2021). https://doi.org/10.1140/epjp/s13360-021-01205-5.

[12] Worldometer. https://www.worldometers.info/coronavirus/. Accessed on September 9, 2022.

[13] B. Tang, X. Wang, Q. Li, et al. Estimation of the transmission risk of the 2019-nCoV and its implication for public health interventions, J. Clin. Med. 9 (2020), 462. https://doi.org/10.3390/jcm9020462.

[14] D.S. Hui, E. I Azhar, T.A. Madani, et al. The continuing 2019-nCoV epidemic threat of novel coronaviruses to global health — The latest 2019 novel coronavirus outbreak in Wuhan, China, Int. J. Infect. Dis. 91 (2020), 264–266. https://doi.org/10.1016/j.ijid.2020.01.009.

[15] S.E. Eikenberry, M. Mancuso, E. Iboi, et al. To mask or not to mask: Modeling the potential for face mask use by the general public to curtail the COVID-19 pandemic, Infect. Dis. Model. 5 (2020), 293–308. https://doi.org/10.1016/j.idm.2020.04.001.

[16] S. Cakan, Dynamic analysis of a mathematical model with health care capacity for COVID-19 pandemic, Chaos Solitons Fractals. 139 (2020), 110033. https://doi.org/10.1016/j.chaos.2020.110033.

[17] B. Buonomo, Effects of information-dependent vaccination behavior on coronavirus outbreak: insights from a SIRI model, Ricerche Mat. 69 (2020), 483–499. https://doi.org/10.1007/s11587-020-00506-8.

[18] Z. Memon, S. Qureshi, B.R. Memon, Assessing the role of quarantine and isolation as control strategies for COVID-19 outbreak: A case study, Chaos Solitons Fractals. 144 (2021), 110655. https://doi.org/10.1016/j.chaos.2021.110655.

[19] S. Olaniyi, O.S. Obabiyi, K.O. Okosun, et al. Mathematical modelling and optimal cost-effective control of COVID-19 transmission dynamics, Eur. Phys. J. Plus. 135 (2020), 938. https://doi.org/10.1140/epjp/s13360-020-00954-z.

[20] O.D. Makinde, J.O. Akanni, A. Abidemi, Modelling the impact of drug abuse on a nation's education sector, J. Appl. Nonlinear Dyn. 12 (2023), 53–73. https://doi.org/10.5890/jand.2023.03.004.

[21] J.O. Akanni, Mathematical assessment of the role of illicit drug use on terrorism spread dynamics, J. Appl. Math. Comput. 68 (2022), 3873–3900. https://doi.org/10.1007/s12190-021-01674-y.

[22] X.P. Li, M.H. DarAssi, M.A. Khan, et al. Assessing the potential impact of COVID-19 Omicron variant: Insight through a fractional piecewise model, Results Phys. 38 (2022), 105652. https://doi.org/10.1016/j.rinp.2022.105652.

[23] P. Kumar, R. Haloi, D. Bahuguna, et al. Existence of solutions to a new class of abstract non-instantaneous impulsive fractional integro-differential equations, Nonlinear Dyn. Syst. Theory, 16 (2016), 73–85.

[24] A. Atangana, D. Baleanu, New fractional derivatives with nonlocal and non-singular kernel: Theory and application to heat transfer model, Therm Sci. 20 (2016), 763–769. https://doi.org/10.2298/tsci160111018a.

[25] Fatmawati, E.M. Shaiful, M.I. Utoyo, A fractional-order model for HIV dynamics in a two-sex population, Int. J. Math. Math. Sci. 2018 (2018), 6801475. https://doi.org/10.1155/2018/6801475.

[26] E. Bonyah, R. Zarin, Fatmawati, Mathematical modeling of cancer and hepatitis co-dynamics with non-local and non-singular kernel, Commun. Math. Biol. Neurosci. 2020 (2020), 91. https://doi.org/10.28919/cmbn/5029.

[27] V.V. Tarasova, V.E. Tarasov, Comments on the article long and short memory in economics: fractional-order difference and differentiation, Probl. Mod. Sci. Educ. 31 (2017), 26–28. https://doi.org/10.20861/2304-2338-2017-113-002.

[28] W. Wang, M.A. Khan, Fatmawati, et al. A comparison study of bank data in fractional calculus, Chaos Solitons Fractals. 126 (2019), 369–384. https://doi.org/10.1016/j.chaos.2019.07.025.

[29] Fatmawati, E. Yuliani, C. Alfiniyah, et al. On the modeling of COVID-19 transmission dynamics with two strains: insight through caputo fractional derivative, Fractal Fract. 6 (2022), 346. https://doi.org/10.3390/fractalfract6070346.

[30] C.W. Chukwu, Fatmawati, Modelling fractional-order dynamics of COVID-19 with environmental transmission and vaccination: A case study of Indonesia, MATH. 7 (2022) 4416-4438. https://doi.org/10.3934/math.2022246.

[31] M. Aychluh, S.D. Purohit, P. Agarwal, et al. Atangana–Baleanu derivative-based fractional model of COVID-19 dynamics in Ethiopia, Appl. Math. Sci. Eng. 30 (2022), 635–660. https://doi.org/10.1080/27690911.2022.2121823.

[32] S. Ahmad, A. Ullah, Q.M. Al-Mdallal, et al. Fractional order mathematical modeling of COVID-19 transmission, Chaos Solitons Fractals. 139 (2020), 110256. https://doi.org/10.1016/j.chaos.2020.110256.

[33] A. Abdelrazec, J. Bélair, C. Shan, et al. Modeling the spread and control of dengue with limited public health resources, Math. Biosci. 271 (2016), 136–145. https://doi.org/10.1016/j.mbs.2015.11.004.

[34] J. Mushanyu, F. Nyabadza, G. Muchatibaya, et al. Assessing the potential impact of limited public health resources on the spread and control of typhoid, J. Math. Biol. 77 (2018), 647–670. https://doi.org/10.1007/s00285-018-1219-9.

[35] I. Podlubny, Fractional differential equations, Vol. 198, Mathematics in Science and Engineering, Academic Press, San Diego, (2010).

[36] J.O. Akanni, F.O. Akinpelu, S. Olaniyi, et al. Modelling financial crime population dynamics: optimal control and cost-effectiveness analysis, Int. J. Dynam. Control. 8 (2019), 531–544. https://doi.org/10.1007/s40435-019-00572-3.

[37] J.O. Akanni, D.A. Adediipo, O.O Kehinde, et al. Mathematical modelling of the co-dynamics of iiiicit drug use and terrorism, Inform. Sci. Lett. 11 (2022), 559–572. https://doi.org/10.18576/isl/110224.

[38] P. van den Driessche, J. Watmough, Reproduction numbers and sub-threshold endemic equilibria for compartmental models of disease transmission, Math. Biosci. 180 (2002), 29–48. https://doi.org/10.1016/s0025-5564(02)00108-6.

[39] S. Olaniyi, J.O. Akanni, O.A. Adepoju, Optimal control and cost-effectiveness analysis of an illicit drug use population dynamics, J. Appl. Nonlinear Dyn. 12 (2023), 133–146. https://doi.org/10.5890/jand.2023.03.010.

[40] A.R.M. Carvalho, C.M.A. Pinto, Non-integer order analysis of the impact of diabetes and resistant strains in a model for TB infection, Commun. Nonlinear Sci. Numer. Simul. 61 (2018), 104–126. https://doi.org/10.1016/j.cnsns.2018.01.012.

[41] K. Diethelm, A.D. Freed, The FracPECE subroutine for the numerical solution of differential equations of fractional order, Forschung und wissenschaftliches Rechnen. 1999 (1998), 57–71.

[42] F.S. Alshammari, M.A. Khan, Dynamic behaviors of a modified SIR model with nonlinear incidence and recovery rates, Alexandria Eng. J. 60 (2021), 2997–3005. https://doi.org/10.1016/j.aej.2021.01.023.